A LINEAR THEORY OF TRANSVERSE CABLE DYNAMICS AT LOW FREQUENCIES

Robert M. Kennedy
Eric S. Strahan
Submarine Sonar Department
Fort Lauderdale Detachment

DTIC
S ELECTE
OCT 2 0 1986
D
D

Naval Underwater Systems Center
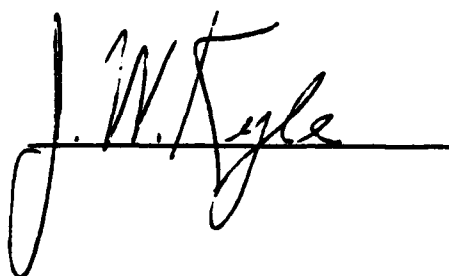## Newport, Rhode Island/New London, Connecticut

86 10 16 377

PREFACE

This report was prepared under Project No. J68028, "Towed Array Motion Studies," Principal Investigator, R. M. Kennedy, Program Manager, J. A. Marsh. The sponsoring activity is the Naval Sea Systems Command, Code 63D, R. Cockerill.

The Technical Reviewer for this report was J. Ianniello.

The authors are grateful for the numerous comments and contributions of Doctors Mark Shensa (NOSC), Paul Rispin (NSRDC), and Jack Ianniello (NUSC). Their inputs and ideas have been used freely throughout the text.

Reviewed and Approved:

J. Kyle
Submarine Sonar Department

The authors of this report are located at the
Central Test and Evaluation Activity,
Naval Underwater Systems Center,
Fort Lauderdale, Florida 33315.

REPORT DOCUMENTATION PAGE		READ INSTRUCTIONS BEFORE COMPLETING FORM
1. REPORT NUMBER TR 6463	2. GOVT ACCESSION NO. AD-A173 3	3. RECIPIENT'S CATALOG NUMBER
4. TITLE (and Subtitle) A Linear Theory of Transverse Cable Dynamics at Low Frequencies		5. TYPE OF REPORT & PERIOD COVERED
		6. PERFORMING ORG. REPORT NUMBER
7. AUTHOR(s) Robert M. Kennedy Eric S. Strahan		8. CONTRACT OR GRANT NUMBER(s)
9. PERFORMING ORGANIZATION NAME AND ADDRESS		10. PROGRAM ELEMENT, PROJECT, TASK AREA & WORK UNIT NUMBERS J68028
11. CONTROLLING OFFICE NAME AND ADDRESS Naval Underwater Systems Center New London Laboratory New London, CT 06320		12. REPORT DATE 5 June 1981
		13. NUMBER OF PAGES 44
14. MONITORING AGENCY NAME & ADDRESS(if different from Controlling Office) Naval Sea Systems Command Washington, DC 20360		15. SECURITY CLASS. (of this report) UNCLASSIFIED
		15a. DECLASSIFICATION/DOWNGRADING SCHEDULE

16. DISTRIBUTION STATEMENT (of this Report)

Approved for public release; distribution unlimited.

17. DISTRIBUTION STATEMENT (of the abstract entered in Block 20, if different from Report)

18. SUPPLEMENTARY NOTES

19. KEY WORDS (Continue on reverse side if necessary and identify by block number)

Ocean Engineering
Towing Hydrodynamics
Cables

20. ABSTRACT (Continue on reverse side if necessary and identify by block number)

This report documents a study of the horizontal motion of the downstream end of a towed cable when the motion of the towing vessel is known. The dynamic position of the downstream end of the cable is a consequence of the random crosstrack meandering of the towing vessel as it imperfectly maintains a constant course. The specific purpose of the study was to supply a method to predict the horizontal motion. Other contributors to cable dynamics, such as ocean current, are not addressed.

DD FORM 1473
1 JAN 73

20.   (Cont'd)

A linear theory for the transverse motion of a cable being towed without purposeful maneuvers was developed.

A cable experiment was then performed at sea to verify the linear theory and to establish parameters that would apply operationally in the sea environment. Specifically, the linear transfer function relating the transverse horizontal motion of the upstream and downstream ends of a long steel cable was calculated and measured.

Finally, the theoretical results were compared with the experimental results. The agreement between the results was reasonable, but not perfect. A more exact treatment of the three-dimensional problem, and/or incorporation of the usual nonlinear hydrodynamic forces, would presumably improve the model. However, the major effort required would result in only a minor improvement.

The results of this study are an improved understanding of the transverse dynamics of long, flexible cylinders in axial flow, and an analytically simple (relative to numerical methods) algorithm for predicting the horizontal motion of a towed vehicle caused by the random crosstrack meandering of the towing vessel.

TABLE OF CONTENTS

QUALITY INSPECTED 1

Accesion For	
NTIS CRA&I	☑
DTIC TAB	☐
Unannounced	☐
Justification	

By ....

Dist.ibution /

Availability Codes	
Dist	Avail a.d/or Special
A-1	

LIST OF ILLUSTRATIONS

INTRODUCTION

GENERAL

Ocean engineers frequently conduct studies in which a surface vessel tows an oceanographic, optical, or acoustic instrumentation package at the end of a long cable. It is important, in such a case, to know the position of the instrumentation package while the vessel attempts to maintain a constant course. The degree of precision needed when predicting this position depends on the task itself. This precision can vary from tens of meters in oceanographic applications to tens of centimeters for some acoustic applications. This report documents the findings of a study undertaken to develop procedures for predicting the position of the instrumentation package towed behind the cable. This study should be viewed as an effort to develop an analytical basis for an optimum linear shape predictor. Such an estimator requires additional information, such as optimal parameter values, instrumentation error characteristics, etc.

In the past, approximate numerical schemes have been used to simulate the dynamic conditions of interest to this study.[1] Numerical techniques require numerical experiments to obtain insight into the physical processes involved. Extensive experimentation is typically not possible because numerical studies require significant computer capability and are tedious and costly. Mudie and Ivers concluded that sinusoidal deviations of the towing ship from a straight towing track resulted in delayed and reduced excursions of the towed package.[1] This result will be commented on extensively in the present work, in which a different approach was taken; explicit solutions of partial differential equations describing the cable dynamics were sought. More specifically, the cable was considered to be a long flexible cylinder in axial flow in a two-dimensional horizontal space. The consequences of the cable being negatively buoyant, and thus occupying depth, the third dimension, were handled in an ad hoc manner by modifying the parameters to account for the horizontal-vertical interaction of forces.

This study comprised an analytical phase and an experimental phase with a resultant data comparison. In the Analytical Program section of this report, the momentum equation developed by Paidoussis[2] and the particular solution suggested by Ortloff and Ives[3] are discussed. Various aspects of the Ortloff and Ives solution are then discussed in detail; the solutions to the particular problem of sinusoidal forcing of the upstream boundary of the cable are discussed first, and then the complementary solution is developed. The complementary solution leads to further discussion regarding the stability of the system. The section concludes by developing a method for modifying the results to incorporate the effects of the non-neutrally buoyant cable. In the Experimental Program section, a cable experiment performed at sea is described; the experiment was designed to verify the theory and to establish parameters that apply operationally in the sea environment. A theoretical experimental comparison discussion follows.

ANALYTICAL APPROACH

Our study began with an examination of the behavior of long, neutrally buoyant cylinders under tow in water; the study was limited to the case in which the cable assumes relatively shallow angles with respect to the flow, which is typical when the tow ship attempts to steer a straight course. We were primarily concerned with the random lateral motion about a straight towing path. The aim of the analytical portion of the study was to solve a momentum equation in order to predict the position of the instrumentation package.

Paidoussis' Equation

The basic approach used the solution suggested by Ortloff and Ives[3] to solve the momentum equation developed by Paidoussis.[2]

We are interested in a momentum equation that describes the dynamics of a long, thin, flexible body in fluid flow. The equation is, necessarily, a nonlinear partial differential equation as a consequence of the nonlinear hydrodynamic forces.[4] Solving this nonlinear equation would be quite difficult, and no one, to date, has attempted it.

Paidoussis, however, suggested that the equation could be linearized when the cable assumed small angles with respect to the flow*. This change from the nonlinear to the linear equation greatly facilitated the development of a solution. Paidoussis based his linearization theory on a modification of the model for hydrodynamic forces suggested by G. I. Taylor[5] in his work on the swimming of eels and worms. However, the basis for the Paidoussis linearization is questionable because of two factors: (1) this modification was not developed for the smooth cylinders of interest to Paidoussis (and to this study), and (2) the form of the hydrodynamic force at shallow angles that allowed for the linearization had not been experimentally verified. Recently, Rispin[6] performed experiments that verified the "small angle" form used by Paidoussis in his linearization and defined the limits over which such a linearization applies. Specifically, it appears that the linear momentum equation derived by Paidoussis applies if the cable-fluid angles do not exceed 2.5 to 3 degrees.

The purpose of the solution, as worked out by Paidoussis, was not to determine shape explicitly, but rather to predict the instabilities that might exist in such a system. Unfortunately, the complexity of even the linearized expression prevents easy interpretation or understanding of the physical process. Numerical analysis of the power series solutions was performed by Paidoussis to identify stability regions and was later extended by Pao.[7]

---

*The concern here is for the dynamically changing cable angle in the horizontal plane. The static vertical depression angle resulting from the weight of the cable will be addressed later.

Pao's Contribution

Pao's[7] stability calculations are also particularly pertinent to this current work. His theoretical and experimental work showed that there are no hydrodynamic instabilities in long cylinders because long cylinders have tensions high enough to filter out the modes of instability, except near the free end (within 20 diameters) where the tensions again become quite small. Pao's results agree with the tow tank observations at the David Taylor Naval Research and Development Center[8], which also showed that no instabilities occur along towed flexible cylinders. The conclusion directed this effort to study motions in towed cylinders that result from external forces on the system, not spontaneous instabilities. Thus, we should expect the cable to respond to forces applied by the tow vessel and/or oceanographic current shears.

Previous Attempts to Solve Paidoussis' Equation

Although no one has attempted to solve the full nonlinear momentum equation, several modest attempts have been made to solve the Paidoussis equation with the intention of studying cylinder shape. Pao and Tran[9] used numerical integration schemes to solve the Paidoussis equation with a sinusoidal forcing at the forward end. Only numerical examples were worked out and no general conclusions about the system resulted. Gardner and Lindemann[10] considered the solution for the special case when the ratio of the forcing wavelength to cylinder diameter is small (less than 50). They showed that the motions caused in this case were the same as in a wave system traveling in a "beam"; for high frequencies the flexural rigidity of the cable dominates and thus causes the cylinder to behave like a beam. They also showed that the fluid forces were small relative to the flexural rigidity of the cylinder so that the actual response of the system was similar to that of a beam in a vacuum. However, Gardner's and Lindemann's solution is of little interest to our study because the tow vessel will excite the cable with longer wavelengths as it meanders back and forth randomly across its average course.

An explicit solution to the Paidoussis equation, modified by the omission of the flexural stiffness term, was found by Ortloff and Ives.[3] This solution applies in the parameter region opposite to that addressed by Gardner and Lindemann; the Ortloff and Ives solution assumes that the forcing wavelength is much larger than 50 times the cylinder diameter, thus making the cylinder respond as though it were infinitely flexible. This modification is particularly applicable to this study, in which we are interested in the low frequency crosstrack meandering of a ship towing a cable where forcing wavelengths typically exceed 1000 meters. The principal result of the Ortloff and Ives work was an explicit closed form solution for the cylinder's space-time shape.

Kennedy[11] developed approximate solutions to the Paidoussis equation for low and high frequency excitation of the system by the tow vessel. He determined that the cable responds in three distinct manners over a range of excitation frequencies. At low frequencies, the cable is dominated by hydrodynamic forces that cause deformations put into the cable by the

towing vessel to propagate downstream relatively unattenuated and with a propagation speed near the tow speed. As the frequency increases, the inertial forces and tension stiffness of the cable become important and wave systems typical of string waves are produced. These waves have a phase velocity that diminishes as the wave proceeds toward the free end as a consequence of the diminishing tension. Finally, at high frequencies, the response of the cable is dominated by the flexural rigidity of the cable and the "beam in a vacuum" response noted by Gardner and Lindemann is reproduced. This present study goes beyond the approximate solutions of Kennedy's work[11] to develop an analytically more exact solution.

ANALYTICAL PROGRAM

GOVERNING EQUATION

The basic partial differential equation (PDE) applied in this study was derived and discussed in several papers.[2,3,11] The equation describes the dynamics of the physical configuration (see figure 1) that consists of a flexible cylindrical body of circular cross section, immersed in an incompressible fluid of uniform density which is flowing* with uniform velocity (U) parallel to the x axis.[2] The equation is expressed as:

$$(M+m) \frac{\partial^2 y}{\partial t^2} + MU^2 \frac{\partial^2 y}{\partial x^2} + 2MU \frac{\partial^2 y}{\partial x \partial t} - \frac{\partial}{\partial x}\left[2c_t \frac{M}{d_c} U^2(L-x) \frac{\partial y}{\partial x}\right]$$

$$+ 2c_t' MU^2 \frac{\partial^2 y}{\partial x^2} + \frac{2c_n}{\pi} \frac{M}{d_c} U\left(\frac{\partial y}{\partial t} + U \frac{\partial y}{\partial x}\right) = 0 ,$$
(1a)

where

$y(x,t)$ = crosstrack position of the cylinder measured at x,

x = along track independent space variable increasing downstream,

t = time,

M = effective mass of fluid "pushed" by the cylinder per unit length of cylinder,

m = mass of the cylinder per unit length,

U = free stream velocity,

L = cylinder length,

d_c = cylinder diameter,

c_t = tangential (longitudinal) drag coefficient,

c_t' = drag coefficient added to account for a drogue at the end of the cable, and

c_n = coefficient of the linearized normal drag expression.

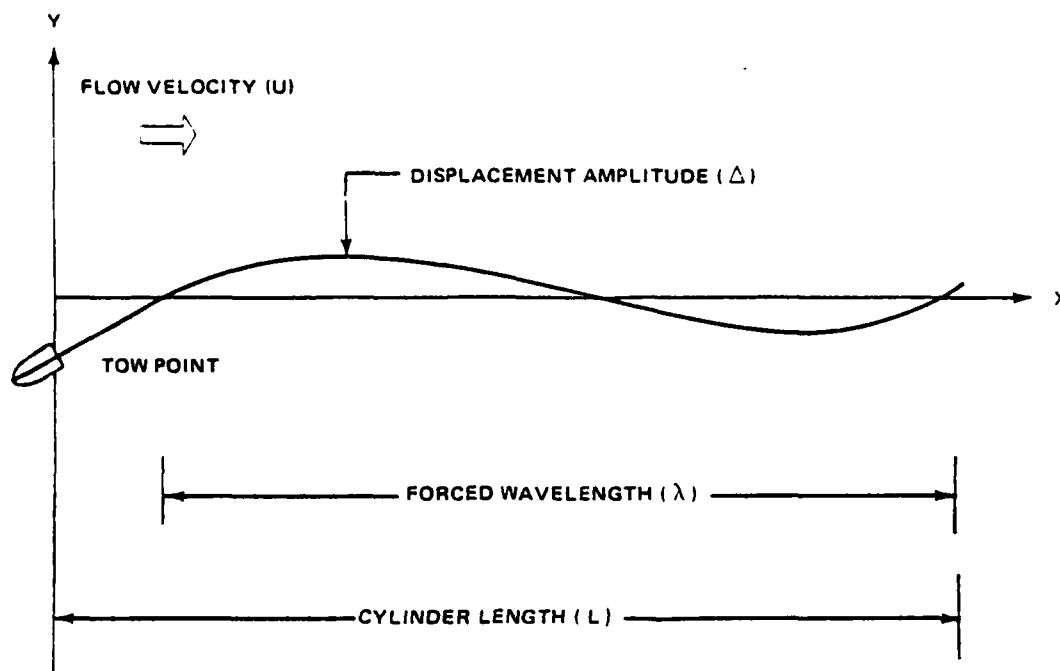*Or equivalently, being towed with uniform velocity U.

Figure 1. Towing System Coordinates

Equation (1) is the Paidoussis[2] equation with the following modifications and clarifications:

1. The fourth-order spatial derivative describing the transverse force due to the cable's flexible rigidity was neglected. As a rule of thumb, this assumption is appropriate for a cylinder with a diameter (d_c) less than 2 percent of the deflection wavelength.

2. The form of the normal hydrodynamic force (sixth term) is a result of the Paidoussis linearization discussed in the introduction. Laboratory measurements by Rispin[6] indicate that this form is appropriate for cable/flow angles of less than 2.5 to 3 degrees.

3. The form of the hydrodynamic drag coefficients (c_t, c_t', and c_n) was changed to be the same as that typically found in modern literature and defined by the normal and tangential drag forces expressed by:

$$F_t = \frac{\rho}{2} d_c \pi c_t v_t^2 \quad \text{and} \quad F_n = \frac{\rho}{2} d_c c_n v_n^2 \ , \tag{1b}$$

where v_t and v_n are the components of U tangential and normal to the cylinder respectively; ρ is the fluid density. The relation between these drag coefficients and those used by Paidoussis, Ortloff, and Ives is

$$c_N = \frac{4}{\pi} c_n \quad \text{and} \quad c_T = 4c_t \ , \tag{1c}$$

where c_N and c_T are the Paidoussis coefficients.

The following nondimensional variables were introduced into equation (1):

$$\tau = \frac{t}{L} U , \quad \xi = \frac{x}{L} , \quad \eta = \frac{y}{\Delta} , \quad \beta = \frac{M}{M+m} , \quad \epsilon = \frac{L}{d_c} , \quad \text{and} \quad \omega = 2\pi f \frac{L}{U} , \quad (2)$$

where f is a frequency variable and Δ is an arbitrary length which can take on any value since equation (1) is linear in y. (Later, Δ will be identified with the magnitude of the forced vibration.) The result is

$$\frac{\partial^2 \eta}{\partial \tau^2} + 2\beta \frac{\partial^2 \eta}{\partial \tau \partial \xi} + (a+b\xi) \frac{\partial^2 \eta}{\partial \xi^2} + c \frac{\partial \eta}{\partial \xi} + d \frac{\partial \eta}{\partial \tau} = 0 , \quad (3)$$

where

$$a = \beta \left(1 - 2c_t \epsilon - 2c_t' \right) ,$$
$$b = 2\beta c_t \epsilon ,$$
$$c = 2(c_t + c_n/\pi)\epsilon\beta , \text{ and}$$
$$d = (2/\pi)\beta c_n \epsilon .$$

The fundamental properties of the solutions of the PDE of equation (3) depend on the type of PDE (i.e., hyperbolic, parabolic, elliptic).* The type, in turn, depends on the roots of the radical as shown:

$$\left[\beta^2 - (a+b\xi) \right]^{1/2} .$$

Since β is small, approximately 1/2, the behavior of the solutions of equation (3) is critically dependent on the sign of the coefficient of the second-order space derivative expressed by:

$$a+b\xi = \beta \left[1 - 2c_t' - 2c_t \epsilon(1-\xi) \right] .$$

As discussed later, $a+b\xi$ is typically less than zero for most of the length of the cylinder, yielding real roots of the radical. Hyperbolic systems of PDE's have real roots and correspond to solutions for which disturbances on the boundaries and at initial conditions propagate along the cylinder.

A typical value of $2c_t\epsilon$ is 10^2, meaning that with no drogue or instrument drag the PDE will be hyperbolic at the upstream end and remain so over better than 99 percent of its length. The addition of drogue or instrument drag could easily make the PDE hyperbolic over its entire length. The physical significance of this is that the boundary disturbances at $\xi = 0$ will propagate aft over most of the cable's length.

---

*A discussion of PDE types and their characteristics may be found in any text that covers partial differential equations.

In solving the equation, we make the fundamental assumption that the solution of $\eta(\xi,\tau)$ is separable in space and time, and the time dependence is harmonic; that is,

$$\eta(\xi,\tau) = v(\xi)e^{i\omega\tau} , \tag{4}$$

where ω is noted to be nondimensional and, in general, complex* and i denotes the imaginary number.

Substituting equation (4) into equation (3), along with the transformation of the independent spatial variable ($z^2 = a+b\xi$), yields the ordinary differential equation (ODE)

$$\frac{d^2v}{dz^2} + \frac{a_0}{z}\frac{dv}{dz} + b_0^2 v = 0 , \tag{5}$$

where

$$a_0 = \frac{2}{b}(c + 2i\omega\beta) - 1 \text{ and}$$

$$b_0^2 = \frac{4\omega}{b^2}(id-\omega) .$$

Equation (5) is recognized as a modified form of Bessel's equation.[4]

PARTICULAR SOLUTION

To arrive at the particular solution, two required boundary conditions are imposed for this second-order equation. At the upstream end of the cylinder ($\xi = 0$), we impose the first condition on the PDE. For $\xi = 0$ where ω_0 is constrained to be real,

$$\eta(\xi,\tau) = \cos \omega_0\tau .$$

Substitution into equation (4) yields the following for $z^2 = a$,

$$\text{Re}\left[v(z)\right] \cos \omega_0\tau - \text{Im}\left[v(z)\right] \sin \omega_0\tau = \cos \omega_0\tau ,$$

or

---

*The nondimensional angular frequency of ω will be equated to the real nondimensional frequency of ω_0 when we seek the particular solution to a forced vibration problem. However, in the complementary solution the infinite set of Eigen frequencies is necessarily complex as will be shown.

$$\text{Re}\left[v(z)\right] = 1$$
$$\text{Im}\left[v(z)\right] = 0 \ .$$

Note that this condition enters a forcing function through a boundary condition. It is the cylinder response to this forcing that is the basic output of this study since, as discussed in the introduction, long cylinders are stable except, possibly, near the low tension end. We will return to this point in our discussion of the complementary solution.

For a boundary condition on the downstream end of the cable ($\xi = 1$), we encounter a fundamental problem that is a consequence of dropping the flexural rigidity term in the Paidoussis momentum equation. Since the physical constraint at the free end involves bending moments, the second-order system (which allows no bending moments) is unable to characterize the free end physical condition. Analytically, this problem results from changing from a fourth-order to a second-order description. A complete solution would require matching the fourth- and second-order solutions in the resulting "boundary layer" at the free end. This "boundary layer" will only apply to a very short region near the free end. We will not attempt this here, but will seek another physical constraint which is occasionally used in this type of problem. Thus we will require that the lateral cylinder displacement be bounded; that is, for $0 \leq \xi \leq 1$,

$$\eta(\xi,\tau) < \infty \ .$$

To reiterate, we seek the particular solution of the ODE. For $a \leq z^2 \leq (a+b)$,

$$\frac{d^2 v}{dz^2} + \frac{a_o}{z}\frac{dv}{dz} + b_o^2 v = 0 \qquad (6a)$$

under the conditions that for $z^2 = a$,

$$v(z) = 1$$

$$\qquad (6b)$$

and, for $a \leq z^2 \leq (a+b)$, $v(z)$ remains bounded.

The range of z given above covers the entire length of the cylinder; that is, $0 \leq \xi \leq 1$.

The entire solution of $v(z)$ can be written as the sum of the particular (v_1) and complementary (v_2) solutions; that is,

$$v(z) = v_1(z) + v_2(z) \ . \qquad (7)$$

The complementary solution is addressed in the next section. The development of the particular solution follows.

Ortloff and Ives recognized that a complete solution set is*

$$v(z) = z^{\nu} \left[A J_{\nu}(b_o z) + B J_{-\nu}(b_o z) \right] \tag{8a}$$

for all values of the complex order

$$\nu = \frac{1-a_o}{2} = 1 - \frac{1}{b}\left(c + i 2\beta\omega\right)$$

or

$$\nu = 1 - \frac{c_t + (1/\pi)c_n}{c_t} - i \frac{\omega}{c_t \epsilon} = -\frac{c_n}{\pi c_t} - i \frac{\omega}{c_t \epsilon} \quad .$$

For all cases of interest to this report, the order is approximated as real as expressed by:

$$\frac{|\omega|}{c_t \epsilon} \ll \frac{c_n}{\pi c_t} \quad , \tag{8b}$$

which limits the analysis to frequencies much less than $\epsilon c_n/\pi$.

Bessel functions of complex order are numerically difficult to evaluate, and thus their use in this report would significantly increase computational efforts. Thus the region of inquiry is limited to that for which the approximation

$$\nu \simeq -p \quad \text{and} \quad p = \frac{c_n}{\pi c_t} > 0 \tag{8c}$$

is appropriate. (Note that the constraint required limits the maximum value that nondimensional ω can obtain. This is consistent with our previously implied low frequency constraint which resulted from neglecting the flexural rigidity term.) The solution may then be written as

$$v(z) = z^{-p} \left[A J_{-p}(b_o z) + B J_p(b_o z) \right] . \tag{9}$$

We next address the application of the boundedness constraint and the upstream ($\xi = 0$) boundary condition in regard to assigning values to the A and B coefficients of equation (9). Note that $z^{-p} J_{-p}(z)$ and $z^{-p} Y_p(z)$ are both singular when z is zero. Thus, if z is zero in the

---

*For integer values of ν, J_{ν} must be replaced with Y_{ν} where J_{ν} and Y_{ν} are Bessel functions of the first and second kind, respectively.

region $a \leq z^2 \leq a + b$, then the coefficient A must be zero to maintain a finite transverse displacement. The region of z in question is equivalent to the region $0 \leq \xi \leq 1$. From equation (3) we may write

$$\xi = 1 - \frac{1 - 2c_t'}{2c_t \epsilon}$$

for $z = 0$.

Thus z cannot be zero for $0 \leq \xi \leq 1$ when $2c_t' > 1$ or when $(1 - 2c_t')/2c_t\epsilon > 1$, which implies that the value of A depends on the magnitude of the drogue or towed body tension. This turns out not to be so (i.e., A must always be zero for boundedness), and we may avoid this computational difficulty by reasoning as follows: in this problem we model tow-body effects as only adding a constant drag to the cable length of interest. Analytically (for our model) there is no change in either the ODE or the boundary condition between a cable length (L) plus a tow body and a cable length (L) plus an additional length of the original cable that generates the same tension as the tow body. These two cases are arithmetically indistinguishable for our model. It is, of course, understood that physically a tow body is not completely described by a steady drag and that the behavior of the two cases could be different.* However, in our current model there is no difference. We will also assert that $\epsilon c_t \gg 1$ for practical cables. Note finally, that this discussion sheds light on an issue left unresolved by Ortloff and Ives.[3]

We will thus substitute a length of the original cable for the towed package such that the new effective length (L*) becomes

$$L* = L + d_c \frac{c_t'}{c_t} .$$

Equation (3) then becomes

$$a = \beta \left(1 - 2c_t\epsilon - 2c_t' \right) = \beta \left(1 - 2c_t\epsilon* \right)$$

and equation (2) becomes

$$\xi* = \frac{x}{L*} \quad \text{and} \quad \epsilon* = \frac{L*}{d_c} .$$

We now seek a solution bounded in the region $0 \leq \xi* \leq 1$. From equation (3) we have

---

*This results from the complex lift and drag forces on the towed body, which we have not modeled.

10

$$\xi^* = 1 - \frac{1}{2c_t \epsilon^*}$$

for z = 0 requiring that, because z must be zero somewhere in the region of $0 \le \xi^* \le 1$, A must therefore be zero for finite transverse motion of the lengthened cable.

The preceding discussion justified making A zero in general and in no way modified the value of the solution for $0 < x < L$. We thus return to the original parameter values of equations (2) and (3) and note that equation (9) becomes

$$v(z) = Bz^{-p}J_p(b_o z) \ . \tag{10}$$

Before evaluating the coefficient B (a trivial matter), let us consider the properties of the above solution.

The values of the solution, like the values of a Bessel function with a complex argument, are quite sensitive to the values of the argument. We are concerned with the range and values of the complex quantity, $b_o z$. From equation (5b) we may write

$$b_o z = \pm \frac{2\omega_o^{1/2}}{b^{1/2}} \sqrt{i \frac{d}{b} - \frac{\omega_o}{b}} \ z \ . \tag{11a}$$

Substituting parameter values for the b and d coefficients from equation (3b) yields

$$b_o z = \pm \frac{2\omega_o^{1/2}}{b^{1/2}} \sqrt{i \frac{c_n}{\pi c_t} - \frac{\omega_o}{2\beta c_t \epsilon}} \ z \ .$$

To the same level of approximation as was required to make the Bessel function index real, we have from equation (8b)

$$b_o z \simeq \pm \sqrt{\frac{4\omega_o p i}{b}} \ z \ ,$$

which becomes

$$b_o z \simeq \pm \sqrt{\frac{4\omega_o p}{b}} \ e^{i(3\pi/4)} z$$

for $z^2 < 0$, \hfill (11b)

$$\simeq \pm \sqrt{\frac{4\omega_o p}{b}} \ e^{i(\pi/4)} \ z$$

for $z^2 > 0$. Note that the choice of sign in equation (11) is unimportant because of the symmetry of the basic ODE in equation (5) to b_0 and z.

Figure 2 is a plot of the real and imaginary values of the argument, $b_0 z$, in equation (11a) as the frequency (ω_0) and space (ξ) variables are changed. The solid lines illustrate the values of $b_0 z$ at the upstream ($\xi = 0$) and downstream ($\xi = 1$) boundaries as ω_0 is increased. The dotted line is the locus of values of $b_0 z$ for a constant ω_0 and ξ changing from 0 to 1. Note that the figure is for the case in which

$$z^2 < 0$$

for $\xi = 0$, and

$$z^2 > 0$$

for $\xi = 1$. The range of values for $b_0 z$, which is consistent with the assertion of equation (8b) that is, equation (11b), is shown by the straight line portion of the solid line. Also shown in figure 2 is the position of the system poles (Eigenvalues) as derived in the next section of this report. For the range of ω_0 for which equation (11b) applies, the argument $b_0 z$ is well removed from any resonant effects as is seen by the separation of the values of $b_0 z$ and the system poles in figure 2.

Evaluation of equation (10) for the frequency range of ω_0 for which equation (11b) applies, results in shapes $v(z)$ that always oscillate and decay as ξ goes from 0 to $-a/b$, if $-a/b$ is less than one, and from 0 to 1, if $-a/b$ is greater than one. For typical parameter values of interest, $-a/b$ is approximately equal to or greater than unity.

It is instructive to analyze the small argument case $(b_0 |z| \ll 1)$, which would occur at small frequencies of $\omega \ll d$, by evaluating equation (10) using the first term of the defining power series for a Bessel function.[12] This gives the equation

$$v(z) \simeq B \frac{(\omega d)^{p/2}}{b^p \Gamma(p+1)} e^{i(p\pi/4)} \tag{12}$$

for $0 \le \xi \le 1$, where $\Gamma(\ )$ denotes a gamma function. Equation (12) simply states that at a very low frequency the entire cylinder duplicates, without delay, the motion of the tow point ($\xi = 0$). Incorporating the second term of the defining power series yields

$$v(z) = B \frac{(\omega d)^{p/2}}{b^p \Gamma(p+1)} e^{i(\pi p/4)} \left[1 - i \frac{\Gamma(p+1)}{\Gamma(p+2)} \frac{\omega d}{b^2} (a+b\xi) \right] . \tag{13}$$

The term in brackets may be approximated as

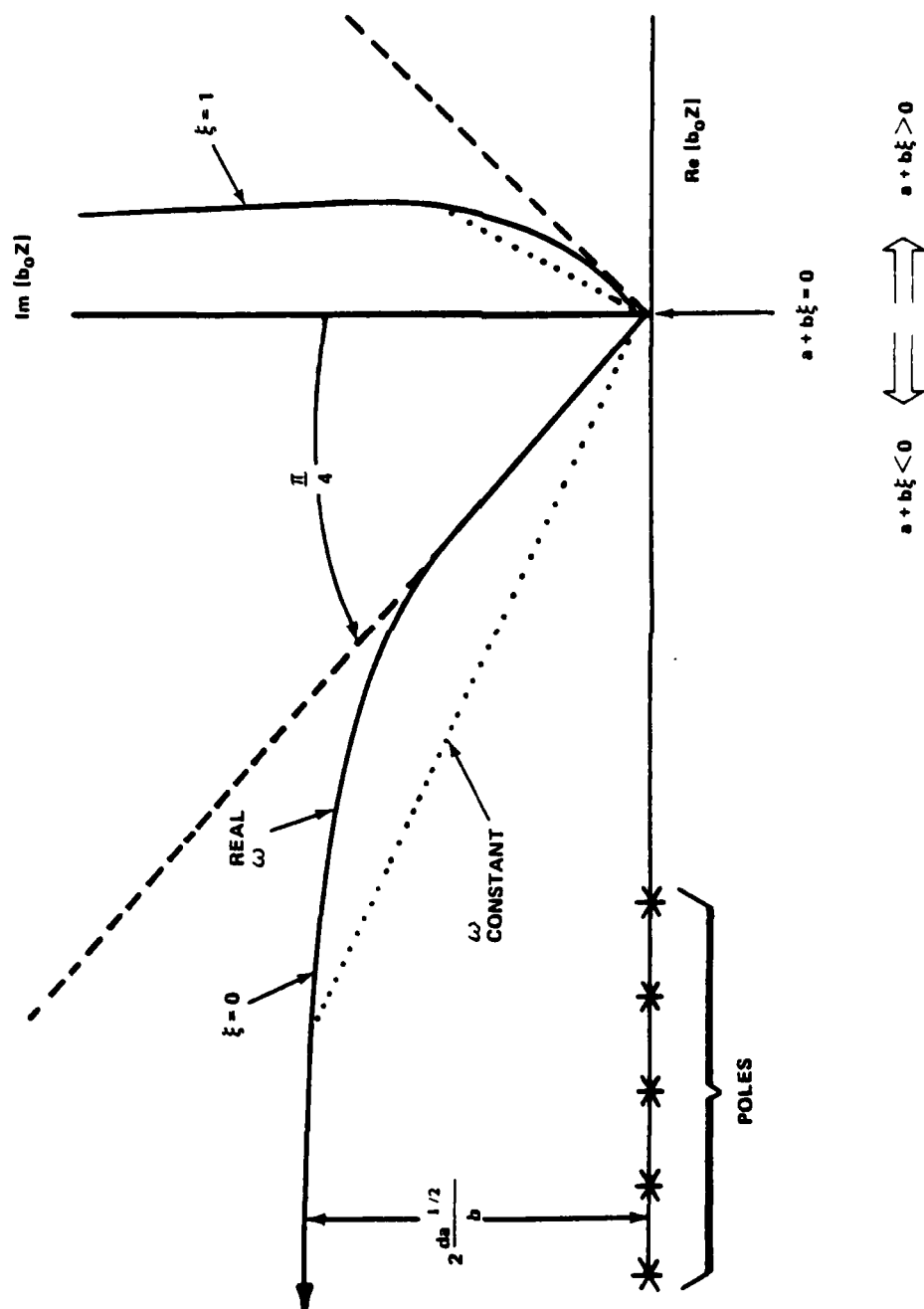$$\exp\left[-i(\phi_1 + \phi_2 \xi) \right] ,$$

12

Figure 2. Bessel Function Arguments

where

$$\phi_1 = \frac{\omega a d}{b^2(p+1)}$$

$$\phi_2 = \frac{\omega d}{b(p+1)} \ .$$

Substituting the values of equations (3b) and (8c) into the above expression for ϕ_2 shows that equation (13) represents a one-dimensional wave propagating downstream with no attenuation and a nondimensional phase speed of

$$c = \frac{(c_n/\pi c_t) + 1}{c_n/\pi c_t} \ . \tag{14}$$

This is the "water pulley" effect described by Kennedy.[11]

Now let us complete the particular solution of equation set (6) by evaluating the complex constant B from equation (10) using the boundary condition of equation (6b).

$$B = \frac{a^{p/2}}{J_p(b_o a^{1/2})} \ , \tag{15}$$

which allows the particular solution to be written as follows. For $a \le z^2 \le a+b$,

$$v_1(z) = \left(\frac{z}{a^{1/2}}\right)^{-p} \frac{J_p(b_o z)}{J_p(b_o a^{1/2})} \ . \tag{16}$$

COMPLEMENTARY SOLUTION

The complementary solution results from solving equation (6a) with the boundary conditions

$$v_2(z) = 0 \tag{17a}$$

for $z^2 = a$, and $v_2(z)$ remains bounded for

$$a \le z^2 \le a+b \ . \tag{17b}$$

Equation (10) is the solution. Thus, with the upstream boundary condition in equation (17), we require that $b_o a^{1/2}$ be equal to the zeros of the

Bessel function of order p. Since Bessel functions with a positive real index are real,[12] we may write this equation as follows. For $n = 1, 2, \ldots$,

$$\delta_n = b_o a^{1/2} , \tag{18}$$

where δ_n are the infinite real zeros of $J_p(b_o a^{1/2})$. The complex frequencies required to meet the boundary condition of equation (17) may be found by substituting equation (5) into equation (18) and solving for the Eigen frequencies (ω_n) as follows:

$$\omega_n = \frac{id}{2} \pm \frac{1}{2} \left(-d^2 - \frac{b^2}{a} \delta_n^2 \right)^{1/2} . \tag{19}$$

Let us examine the Eigen frequencies by substituting equation (3b) into equation (19). After some manipulation, the Eigen frequencies may be written as

$$\omega_n = i \frac{\varepsilon \beta c_n}{\pi} \left[1 \pm \left(1 + \frac{(\delta_n/p)^2}{\beta(1-D)} \right)^{1/2} \right] , \tag{20a}$$

where D is a drag term defined as

$$D = 2c_t \varepsilon + 2c_t' .$$

Only the Eigen frequencies that meet the requirement of equation (8b) can be used, that is,

$$\frac{|\omega_n|}{\varepsilon c_t} \ll p .$$

Thus, for each ω_n we must test the following condition

$$\left| i\beta p \left[1 \pm \left(1 + \frac{(\delta_n/p)^2}{\beta(1-D)} \right)^{1/2} \right] \right| \ll p . \tag{20b}$$

This is a very restrictive condition. To illustrate this point we will examine the condition for the first (smallest) zero (δ_1). Examination of equation (20b) shows that if ω_1 does not meet the condition no other zero will either.

The first zero lies in the interval[12]

$$p < \delta_1 < \left[2(p+1)(p+3) \right]^{1/2} .$$

For large p, $\delta_1 \simeq \sqrt{2\ p}$. So, within a factor of two we may write $\delta_1 \simeq p$, and equation (20b) becomes

$$\left| \ i\beta p \left[1 \pm \left(1 + \frac{1}{\beta(1-D)} \right)^{1/2} \right] \ \right| \ll p \ .$$

A systematic evaluation of the above equation reveals that only when $\beta(1-D) \gg 1$ does the Eigen frequency meet the equation (8b) condition.* This statement may be easily generalized to read:

$$\omega_n = i^{\epsilon\beta c_n/\pi} \left[1 - \left(1 - \frac{(\delta_n/p)^2}{\beta(D-1)} \right)^{1/2} \right]$$

for $\dfrac{(\delta_n/p)^2}{\beta(D-1)} \ll 1$ only. This may be simplified to read:

$$\omega_n \simeq i \ \frac{\epsilon c_n}{2\pi} \ \frac{(\delta_n/p)^2}{(D-1)} \tag{21}$$

for $\dfrac{(\delta_n/p)^2}{\beta(D-1)} \ll 1$.

To summarize, all of the Eigen frequencies, which we can calculate, indicate that the system will be temporally stable since the solution consists of a sum of terms in the form

$$B_n z^{-p} \ J_p(\delta_n) e^{i\omega_n \tau} \ , \tag{22}$$

where ω_n is a positive imaginary number.

Of interest to our present study is the damping time associated with each Eigen frequency because this would be the time required for ship maneuvering effects to have died out after assuming a constant average heading. It is useful to define a damping time (τ_o) as

$$\text{Im}\left(\omega_n\right)\tau_o = 1 \ .$$

---

*Note that the fact that β is approximately 1/2 figures into this conclusion.

The slowest mode (i.e., longest time constant) for $\Gamma > 1$, is given by

$$\tau_{max} = \frac{1}{\min\left[\text{Im}(\omega_n)\right]} \quad , \tag{23}$$

where $\min\left[\text{Im}(\omega_n)\right] = \text{Im}(\omega_1)$. The first zero ($\delta_1$) of J_p may be approximated as before as $\delta_1 \simeq p$. From equation (22) we have

$$\tau_{max} \simeq \frac{2\pi(D-1)}{\epsilon c_n} \quad . \tag{24}$$

In real (dimensional) time

$$(\tau_o)_{max} \simeq \frac{2\pi(D-1)L}{Uc_n\epsilon} = \frac{2\pi(D-1)d_c}{Uc_n} \quad . \tag{25}$$

Typical values for these parameters are $c_t = .0025$, $c_n = .07$, $c_t = 57$, $\epsilon = 75000$, $d_c = .01\text{m}$, $U = 3\text{m/sec}$; therefore,

$$(t_o)_{max} \simeq 150 \text{ seconds} \quad .$$

Ortloff and Ives[3] concluded, wrongly, that the cylinder would always be temporally unstable. Lee and D'Appolito[13] corrected Ortloff's and Ives' error and concluded that if some minimum tension were exceeded then the system would be temporally stable. However, neither of these papers tested the Eigen frequencies for conformance with the condition of equation (8b). The above discussion shows that the region identified by Lee and D'Appolito (D < 1) as being unstable is not necessarily so because for that range of tension the order of the Bessel function cannot be approximated as real. Furthermore, some of the Eigen frequencies are not computable because the Bessel function index is required to be real, so no definite temporal stability statement is possible. The point appears to be academic, however, because there is no experimental reason to believe that an instability exists.

ANALYTICAL EXAMPLES

A qualitative display of cylinder dynamics is shown in figures 3 through 5. These figures were obtained by numerically evaluating equations (4) and (16) for a range of values for ξ and τ. The displays show time histories of the particular solution (i.e., the cylinder transverse shape at three different frequencies). In all cases, the sinusoidal boundary condition imposed on the tow point propagates attenuatively back through the cylinder. As expected, the attenuation rate clearly increases with the frequency.
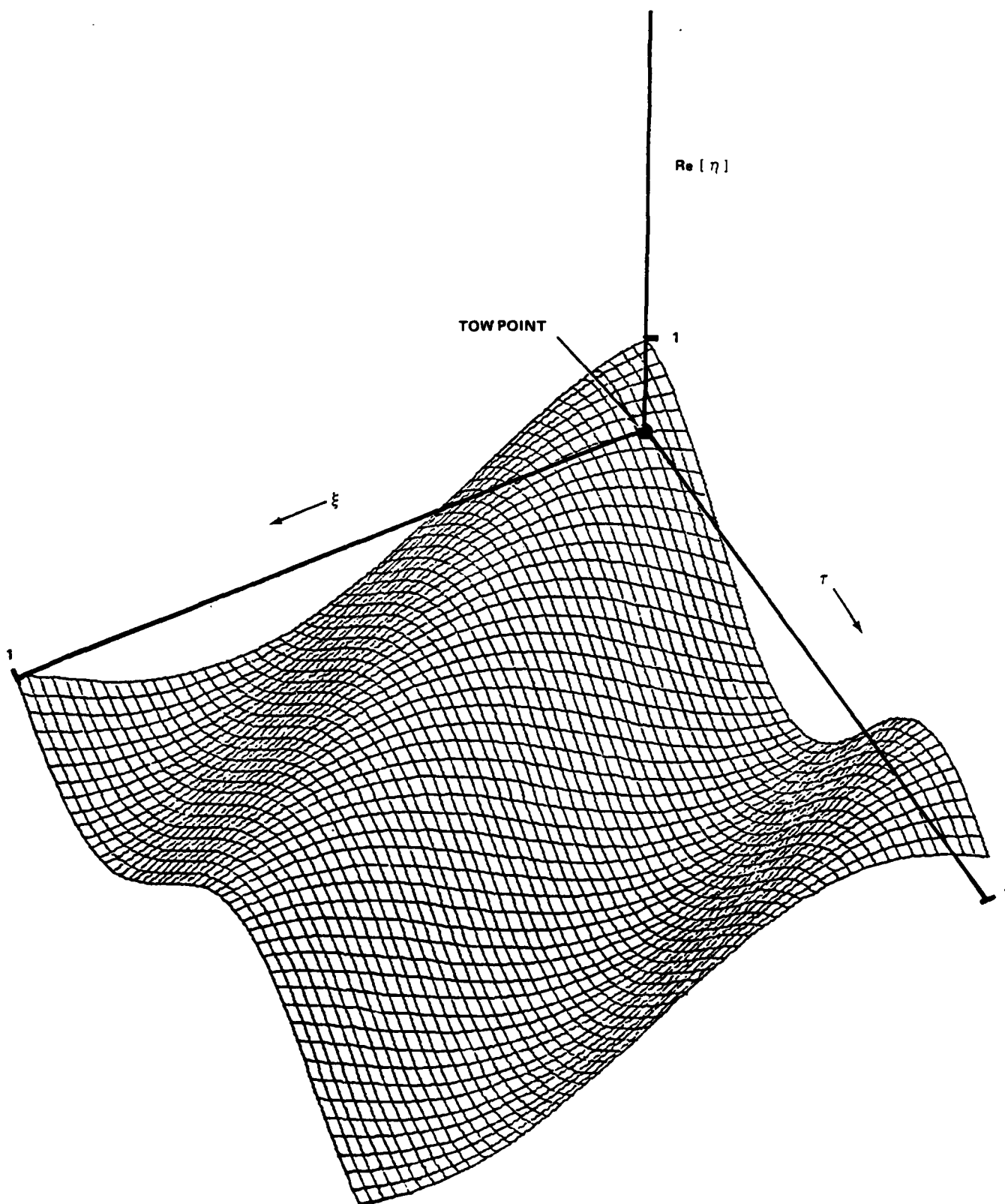
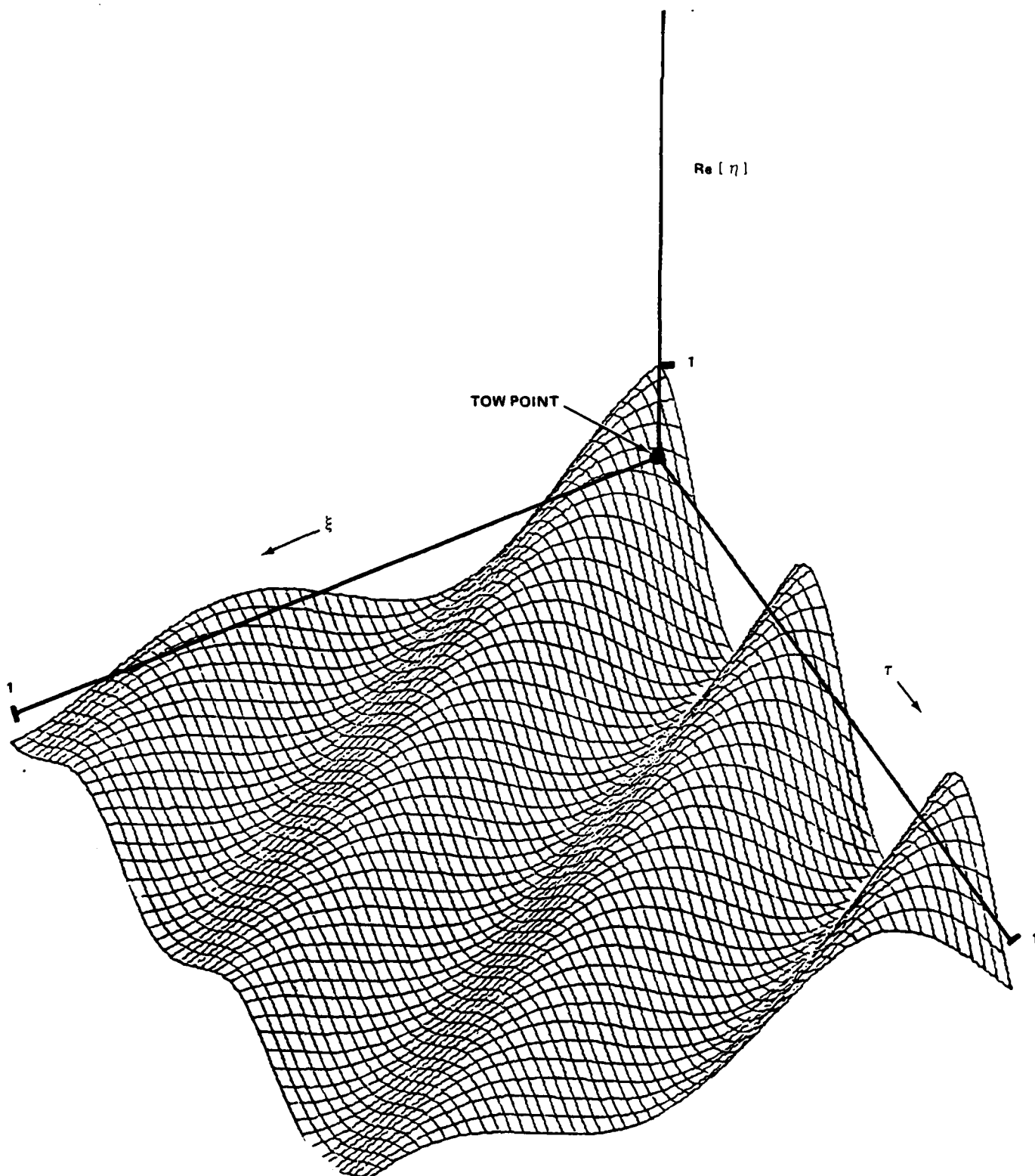**Figure 3. Time History of Cylinder Shape ($\omega = 5$)**

Re $[\eta]$

TOW POINT

ξ

τ

1

1

1

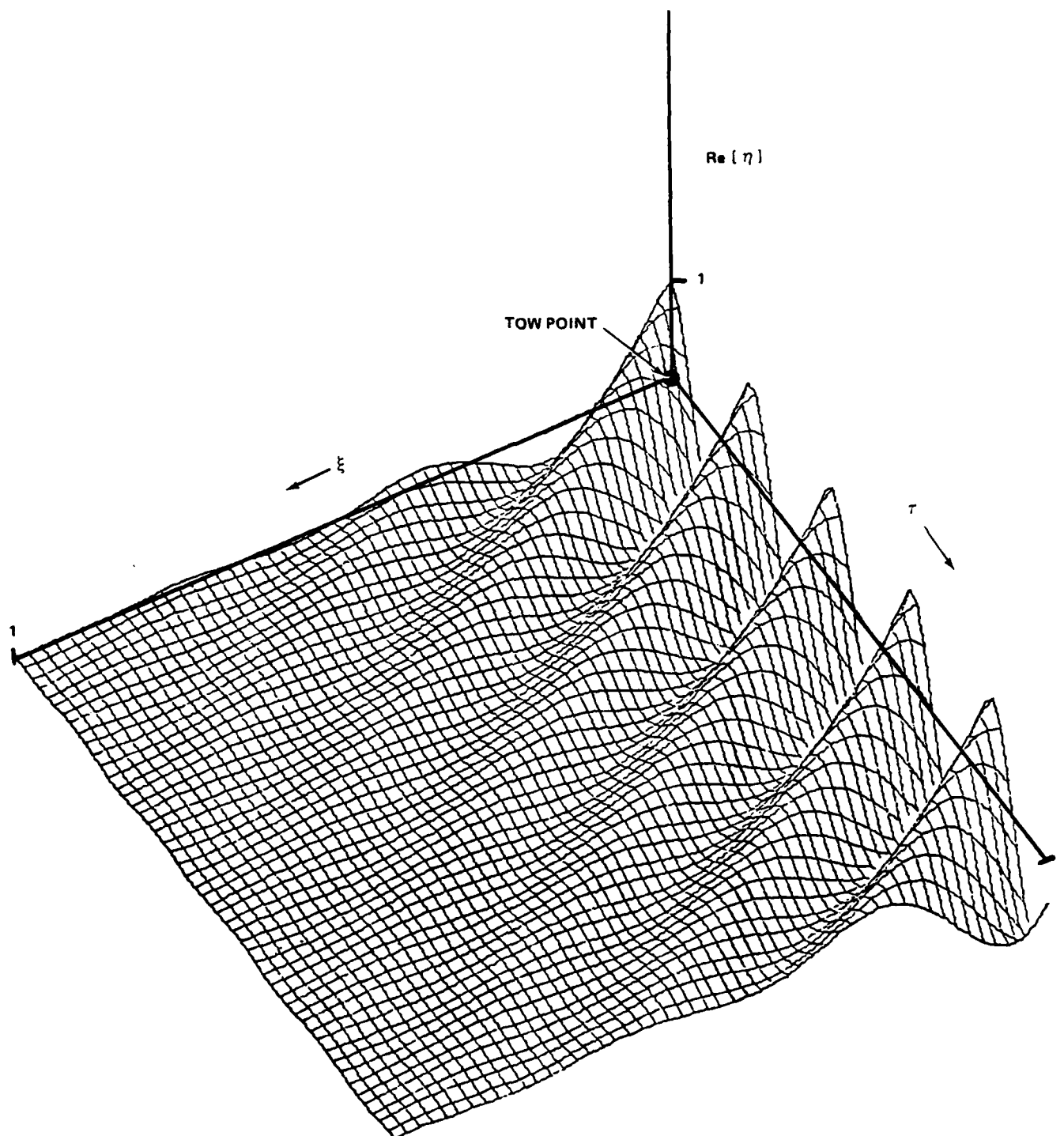Figure 4. Time History of Cylinder Shape ($\omega = 10$)

19

Figure 5.   Time History of Cylinder Shape ($\omega = 20$)

Let us define the transfer function $[H(\omega)]$ to be the complex ratio of the Fourier Transforms of the crosstrack displacements at an arbitrary point on the cylinder (ξ) to the upstream boundary ($\xi = 0$). Using equation (4) this ratio may be written as

$$H(\omega) = \frac{v_1(\xi,\omega_o)}{v_1(0,\omega_o)} ,$$

where, from equation (6b), $v_1(0,\omega_o) = 1$. Thus,

$$H(\omega) = |v_1(\xi,\omega_o)| \, e^{i\psi(\xi,\omega_o)} , \tag{26}$$

where

$$\psi(\xi,\omega_o) = \tan^{-1} \left[\frac{Im(v_1)}{Re(v_1)}\right].$$

The transfer function (ordinate of figure 6) is the ratio of the amplitude of the sinusoidal motion of the cylinder observed at some spatial point (ξ) to that imposed on the cylinder at the forward boundary ($\xi = 0$) for a given frequency (ω_o). From figure 6 we note that the observer at ξ sees the transfer function diminish (from unity) as frequency increases (i.e., the cylinder passes low frequencies and rejects high frequencies).

A point of constant phase obeys $\omega\tau - \psi(\xi) =$ constant. Thus that point will have a velocity given by $\omega d\tau - \psi'd\xi = 0$, and the phase velocity (c) is

$$c = \frac{d\xi}{d\tau} = \frac{\omega}{\psi'} . \tag{27a}$$

Unfortunately, the spatial derivative (ψ') could not be measured directly in the companion experiment described in the next section. Thus we define c* as the phase velocity measured between ξ and ξ equal to zero, as expressed by:

$$c^* = \frac{\omega\xi}{\psi} . \tag{27b}$$

The c* is a function of ξ and ω, requiring a three-dimensional display of the nondimensional phase velocity as given in figure 7. Because of the difficulty of displaying this function, two different viewing angles of the same function are shown in the figure. At low frequencies the nondimensional phase speed is given by equation (14) as $c^* = 1 + p^{-1}$. Typical values of p are greater than 10, which makes c* nearly one and independent of ξ as was predicted by equation (13). As the frequency
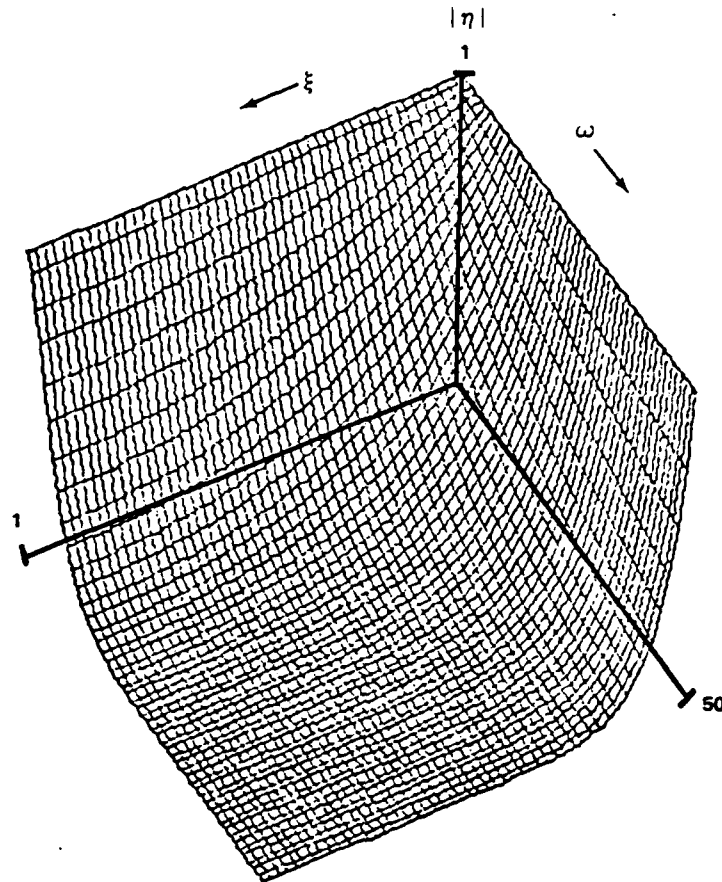
TR 6463

Figure 6. Space Frequency Plot of Transfer Function

increases, c* increases (dispersively) with larger increases occurring nearer $\xi = 0$ than $\xi = 1$. This picture is totally consistent with the physical description given by Kennedy[11] and summarized as follows: at low frequencies the hydrodynamic forces dominate over the cylinder-fluid inertial and cylinder tension stiffness terms, causing the disturbances to propagate downstream at the flow velocity (i.e., c = 1). Because tension stiffness is negligible, the phase velocity is independent of tension and thus independent of ξ. As frequency increases, both the above mentioned forces (inertial and tension stiffness) become important and the cylinder responds with "string-like" waves having propagation velocities greater than flow velocity. The velocity of these waves is proportional to the square root of the cylinder tension and thus decreases as ξ goes from 0 to 1.

HORIZONTAL-VERTICAL INTERACTION

Up to this point in the report we have considered the cable of interest to be a neutrally buoyant flexible cylinder. Actually, most cables are negatively buoyant. Rather than undertake the monumental task of rederiving
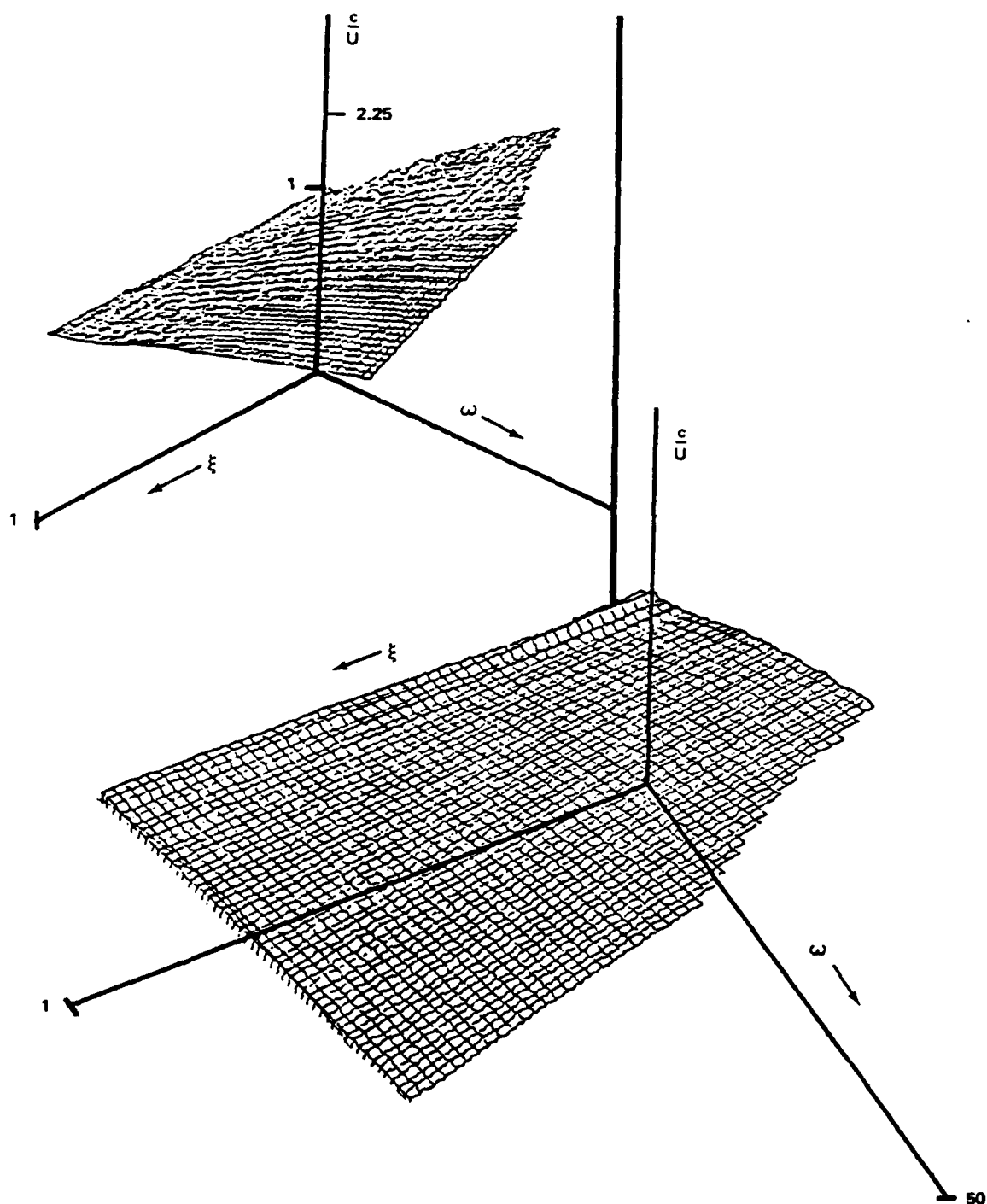
Figure 7.   Space Frequency Plot (Two Views) of
Nondimensional Phase Velocity

and then solving equation (1) in three dimensions, we propose to modify the coefficients of equation (1) to account for the new forces associated with the vertical angle assumed by a negatively buoyant cable.*

Figure 8 illustrates a segment of a cable being towed in the negative y direction, having a horizontal angle with the flow of θ, and having a depression angle φ due to uniform cable weight. The base vector in the cable direction is $\hat{c}$ and may be shown as:

$$\tilde{c} = \hat{i} \sin \theta \cos \phi + \hat{j} \cos \theta \cos \phi + \hat{k} \sin \phi \ , \tag{28}$$

where $\hat{i}$, $\hat{j}$, and $\hat{k}$ are base vectors in a Cartesian coordinate system. The fluid flow vector is

$$\vec{U} = \hat{j}U \ . \tag{29}$$

Figure 8. Horizontal-Vertical Force Diagram

---

*This approach was originally brought to the author's attention by Dr. R. Kronauer of Harvard University.

The tangential and normal components of velocity relative to the cable are found from the following defining equations:

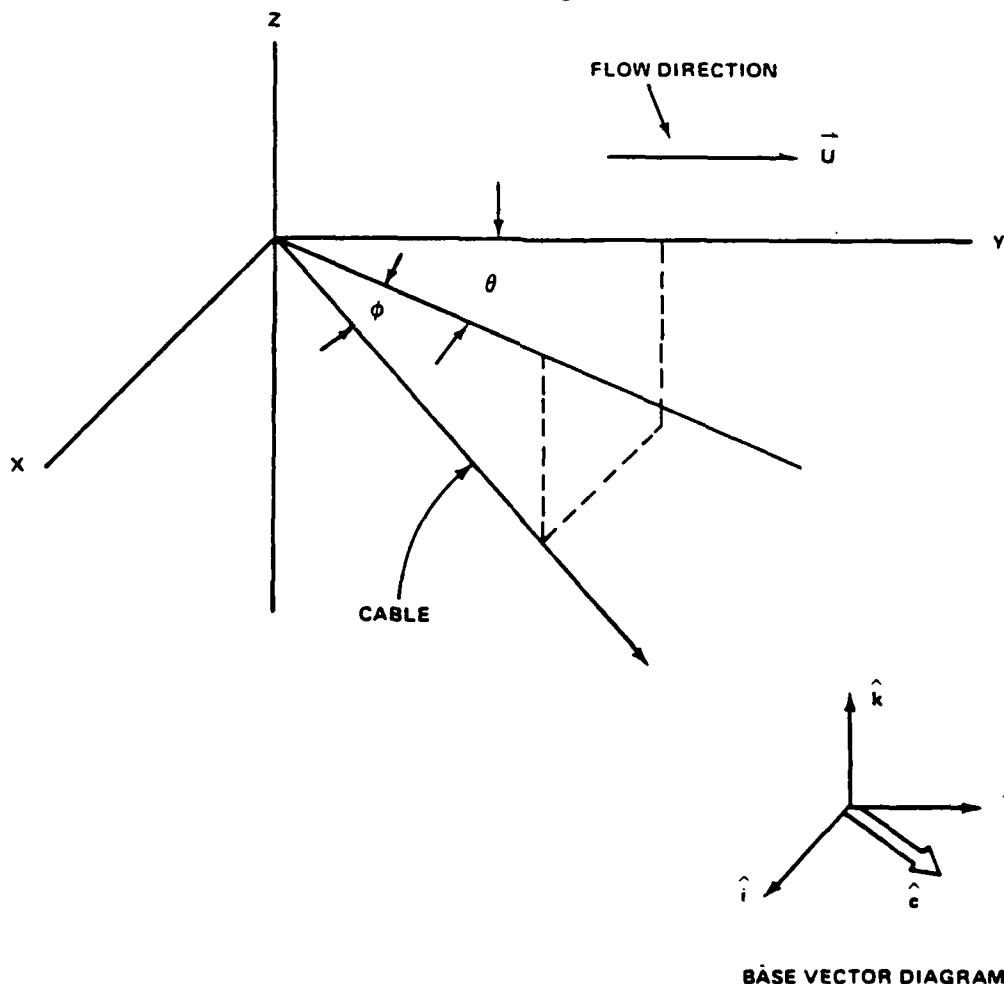$$\vec{U_T} = (\vec{U} \cdot \hat{c})\hat{c}$$

$$\vec{U_N} = \vec{U} - \vec{U_T} \quad . \tag{30}$$

After some tedious but straightforward algebra we may express the normal component of velocity as

$$\frac{\vec{U_N}}{U} = -\hat{i} \cos \theta \cos^2 \phi \sin \theta$$

$$+ \hat{j}(1 - \cos^2 \theta \cos^2 \phi) \tag{31}$$

$$- \hat{k} \cos \theta \cos \phi \sin \phi \quad .$$

The magnitude squared value is

$$\left| \frac{\vec{U_N}}{U} \right|^2 = 1 - \cos^2 \theta \cos^2 \phi \quad . \tag{32}$$

Equations (31) and (32) show that the component of flow normal to the cable is a function of both the horizontal and vertical angles. Thus, the x component of the normal flow, which is what interests us, is also a function of both angles. This means that there is a horizontal force on the cable as a consequence of the vertical angle ϕ. We now proceed to calculate that force. The normal force vector is

$$\vec{F_N} = R(1 - \cos^2 \theta \cos^2 \phi)\hat{n} \quad , \tag{33}$$

where $\hat{n}$ is the base vector normal to the cable (i.e., $\hat{n} \cdot \hat{c} = 0$) and

$$R = \frac{1}{2} \rho c_n d_c U^2 \quad . \tag{34}$$

The quantity n is given by

$$\hat{n} = \frac{\vec{U_N}}{U(1 - \cos^2 \theta \cos^2 \phi)^{1/2}} \quad . \tag{35}$$

To find the horizontal component of force, substitute equation (35) into equation (33) and identify the x component of the result. Again, after some algebra, we have

$$(F_N)_x = -R \cos \theta \cos^2 \phi \sin \theta (1 - \cos^2 \theta \cos^2 \phi)^{1/2} , \qquad (36)$$

which compares with the neutrally buoyant case ($\phi = 0$) of

$$(F_N)_x \mid_{\phi=0} = -R \cos \theta \sin^2 \theta . \qquad (37)$$

$(F_N)_x \mid_{\phi=0}$ is the normal hydrodynamic drag term of equation (1).

A comparison of equations (36) and (37) shows that increasing the depression angle ϕ to about 40 degrees increases the horizontal force by the amplification factor

$$A = \frac{\cos^2 \phi (1 - \cos^2 \theta \cos^2 \phi)^{1/2}}{\sin \theta} , \qquad (38)$$

where

$$(F_N)_x = A(F_N)_x \mid_{\phi=0} .$$

A convenient way to incorporate the amplification of equation (38) into the solution of equation (5) is to increase the coefficient of normal force; that is, c_n^* will be used in place of c_n where

$$c_n^* = A c_n . \qquad (39)$$

Note that singular behavior of A for zero θ has no physical significance since $(F_N)_x$ is zero at zero θ. This is addressed in appendix B.

Physically we have shown in this section that the normal hydrodynamic force on the cable, resulting from a vertical depression angle, will have a horizontal component when the cable is angled to the flow in the horizontal. This describes a horizontal-vertical interaction of forces. The vertical cable angle establishes a flow across the cable that results in a force aligned with the flow in the absence of a horizontal inclination of the cable. However, if the crosstrack meandering of the towing vessel causes a horizontal attack angle on the cable, then the normal force, previously aligned with the flow, is "tipped" in the horizontal direction. Equation (39) modifies the normal drag coefficient to account for this additional horizontal force.

EXPERIMENTAL PROGRAM

DESCRIPTION

During the experimental program, a thin, 16-mm diameter, steel cable was towed from a surface vessel, and the vessel was maneuvered to force sinusoidal horizontal transverse motion at the upstream end of the cable. During each run, the cable was towed through a number of cycles (at least four). Each run was defined by a set of three parameters varied in a factorial type experiment design.[14] The variables were ship speed, the length of cable between the ship and the pinger, and the frequency of the oscillation. These experimental parameters are illustrated in figure 9.

The transverse motions of both the ship and a point on the cylinder were carefully measured by acoustically tracking pingers attached to the ship and the cable at the point to be measured. As shown in figure 10, the tracking was done from spatially fixed hydrophones. The ship maneuvers simulated a sinusoidal upstream boundary condition, and the response of the system (to the stimulation) was measured by the track of the pinger at the end of the cable. A neutrally buoyant cylinder supplied tension (drogue) to the end of the cable.

The objective of the data analysis was to compare the experimental results and the theoretical results discussed in this report. An exact comparison was possible for the magnitude of the transfer function, equation (26), and the phase velocity, equation (27). Experimentally, this was determined by calculating the Fourier transform of the time series of the crosstrack displacements (see figure 9) for both pingers. The transfer function magnitude $|H(\omega)|$ and phase speed (c) were then determined as in equations (26) and (27b) for the single frequency at which the system was forced.

As shown in figure 10, the thin, flexible cable was negatively buoyant as a consequence of the uniform linear weight of the steel cable. Because of the uniform linear weight, the cable tows with a constant depression angle ϕ (called the "critical angle") from the surface down to a depth at which the drogue tension causes the depression angle to transition from ϕ to zero. Knowing the cable length* and the pinger depth from a depth sensor (see figure 10) allows an approximate calculation of the average depression angle as follows

$$\phi \simeq \sin^{-1} \left[\frac{\text{pinger depth}}{L_{c/s}} \right] .$$

This depression angle varied from 4 to 9 degrees during the experiment.[15]

---

*It is important to differentiate between the cable length (Lc/s) of figure 10 and the horizontal projection of cable length (L) of figure 9. It is the length of the cable in the direction of fluid flow (L) which appears in equation (1).

Figure 9. Experimental Parameters

CROSSTRACK

ALONG
TRACK

t = t_0

a = AMPLITUDE

$\frac{2\pi}{k}$

SHIP PATH

DROGUE

CABLE PINGER

TOW CABLE
(THIN FLEXIBLE
CYLINDER)

L

SHIP PINGER

t = t_0 + T

AVERAGE
HEADING

U   = TOW SHIP SPEED

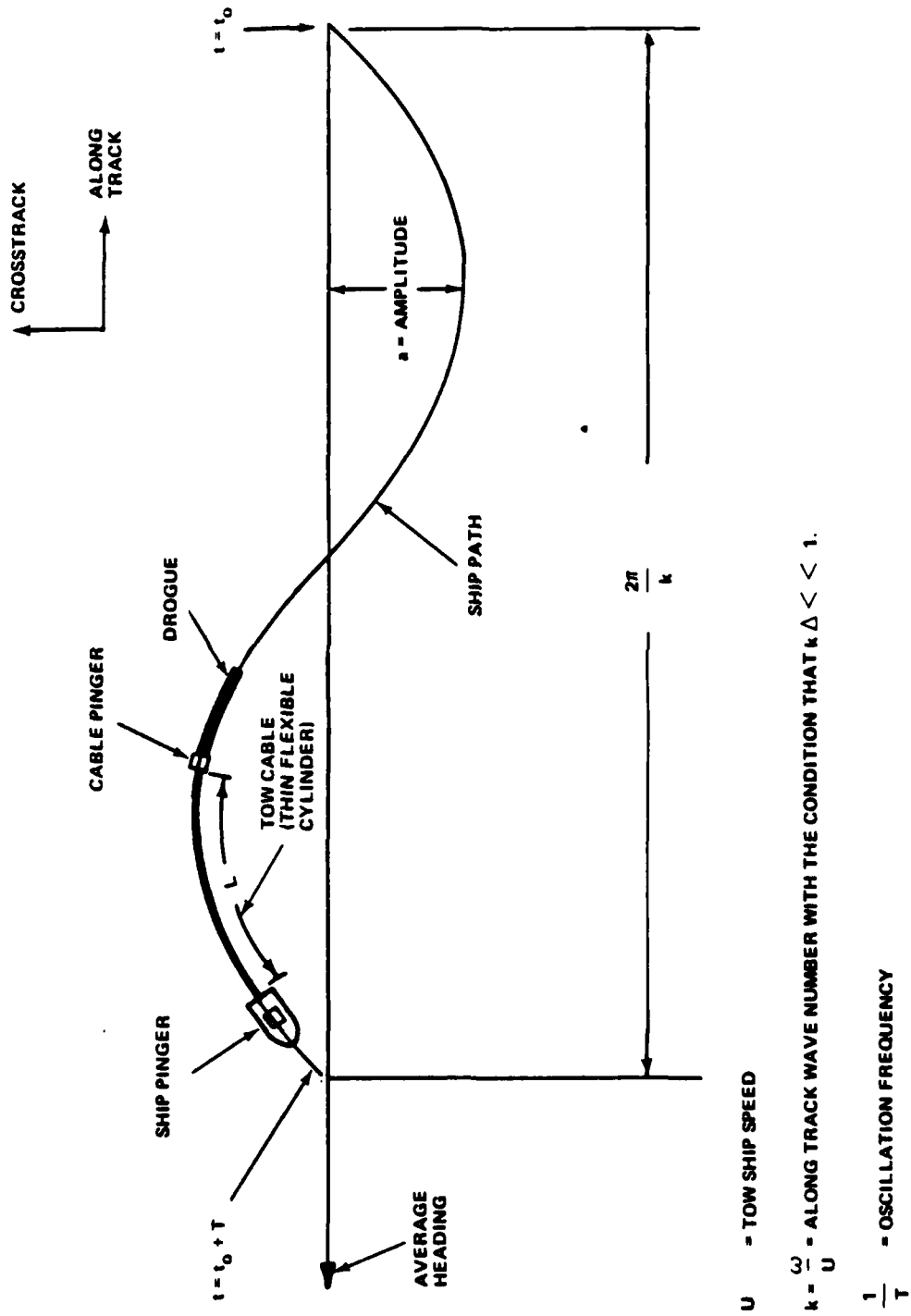$k = \frac{2\pi}{U}$ = ALONG TRACK WAVE NUMBER WITH THE CONDITION THAT k $\Delta \ll 1$.

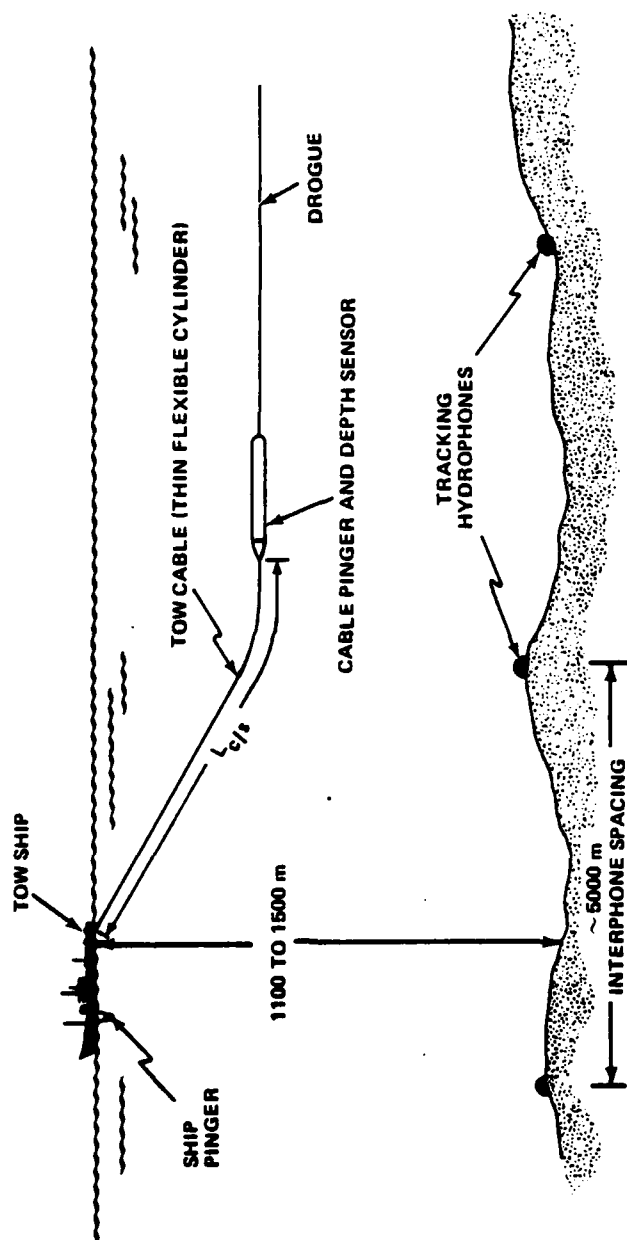$\frac{1}{T}$ = OSCILLATION FREQUENCY

Figure 10. Experimental Configuration

When the experiment was performed, the Rispin[15] results were not available; consequently, the horizontal angle limitations on the Paidoussis linearization were not known (refer to discussion in introduction). Therefore, the angle θ frequently exceeds the 2.5 to 3 degree threshold found by Rispin. Note from figure 9 that θ will vary sinusoidally with a maximum value of ka and an average magnitude of $2/\pi$ka. Experimentally the maximum angles varied from 1.8 to 29.8 degrees, and the average magnitudes varied from 1.1 to 18.9 degrees. From equation (38), it is seen that the amplification of the horizontal force applied to the cable is a function of both θ and ϕ. Figure 11 illustrates the range of amplification that occurs for the experimental range of θ and ϕ cited above. Because θ varies in both space and time, so will the amplification factor. An effective value will be sought experimentally rather than analytically.

Quantitative statements concerning the experimental accuracy will not be made for the following two reasons. The tracking accuracies of the acoustic tracking range are not well understood; this is particularly true regarding how those tracking errors propagate through the data analysis used. Tracking errors represent noise in the process that is not known. In general, estimates of a transfer function based on a finite length time series will contain errors even when the time series contains no noise.[16] This error is a function of both the transfer function to be measured and the test signal used in the measurement. Quantitative evaluation of this error is not trivial and was not undertaken. However, it is thought that neither of these errors will bias the transfer function estimates and that on the average these errors should contribute only random (zero mean) error.

Before an analytical comparison can be made with the data, the "drogue" factor (C_t') needs to be evaluated from the following expression

$$\frac{c_t'}{c_t \varepsilon} = \frac{\text{drag of drogue}}{\text{drag of cable}} \quad .$$

The c_t', from equation (1), accounts for the component of the total drag that is constant over cable length L; i.e., c_t is proportional to the component of tension that varies linearly over L, and c_t is proportional to the component that is constant over L. The drags of the drogue and cable were calculated using the appropriate diameters, lengths, and standard formulas, i.e., equation (1b).

RESULTS

The results of the data analysis are shown in figures 12 and 13. Tables A-1 and A-2 of appendix A summarize the condition of each one of the experimental points for each of the two experiments. The large dots on figure 12 are the experimental values of the transfer function magnitude, previously described, plotted as a function of nondimensional frequency. The dots in figure 13 show the phase velocity, nondimensionalized by the towing speed through the water, also plotted as a function of the nondimensional frequency.
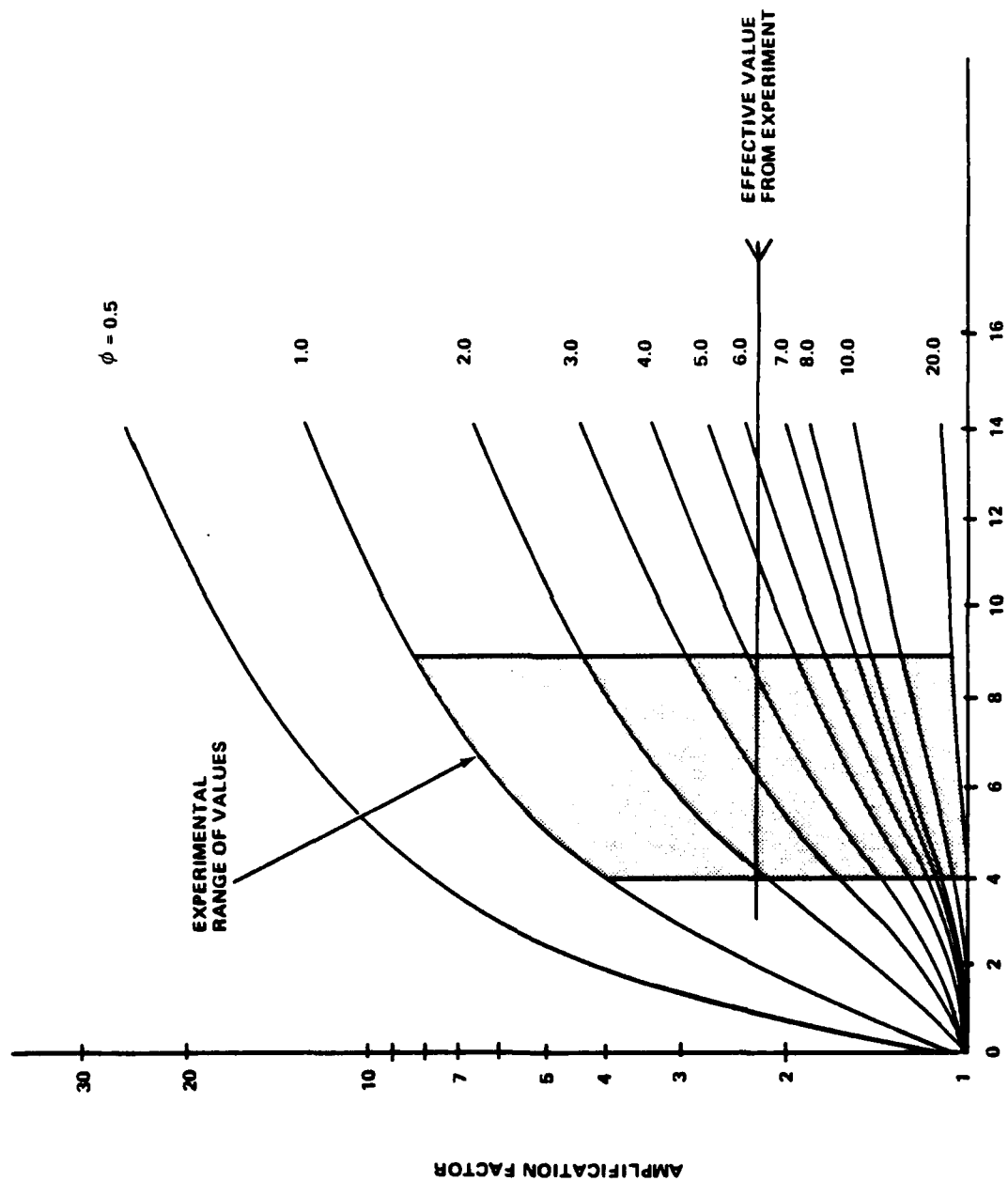
Figure 11. Vertical-Horizontal Interaction Effect

RISPIN NORMAL DRAG COEFFICIENT
MODIFIED FOR CYLINDER DEPRESSION
ANGLE (C_n = .16)

NORMAL DRAG COEFFICIENT
FOR BEST DATA FIT (C_n = .08)

NONDIMENSIONAL FREQUENCY $\left(\dfrac{\omega L}{U}\right)$

TRANSFER FUNCTION MAGNITUDE
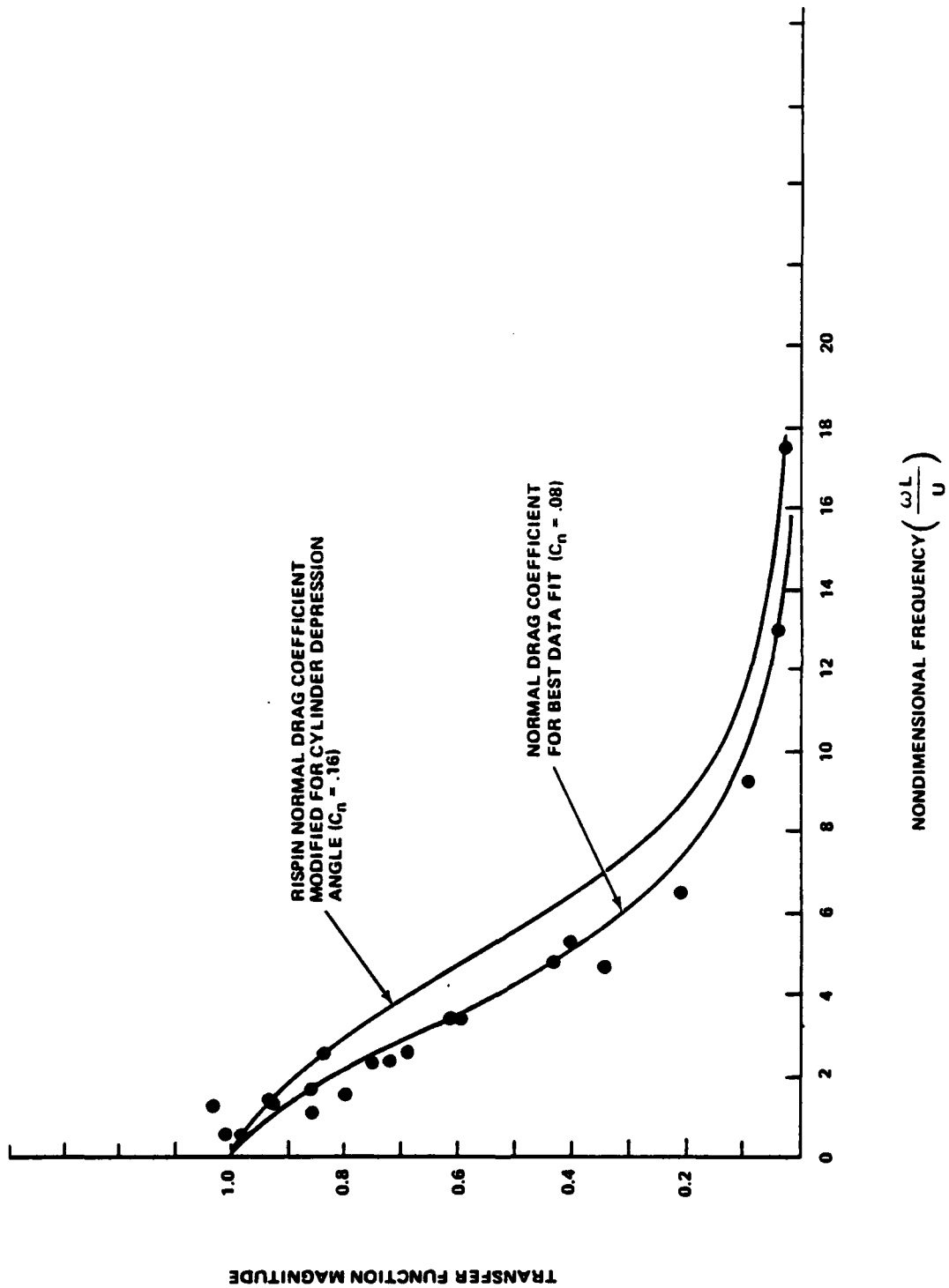
Figure 12. Analytical-Experimental Comparison of
Transfer Function Magnitude

NONDIMENSIONAL FREQUENCY $\left(\frac{\omega L}{U}\right)$

NONDIMENSIONAL PHASE VELOCITY $\left(\frac{c}{U}\right)$

RISPIN NORMAL DRAG COEFFICIENT
MODIFIED FOR CYLINDER DEPRESSION
ANGLE (C_n = .16)

NORMAL DRAG COEFFICIENT
FOR BEST DATA FIT (C_n = .24)

Figure 13. Analytical-Experimental Comparison of Phase Velocity

The solid lines on figures 12 and 13 are theoretical curves resulting from equations (16) and (27b). All of the parameters used in the calculation are reasonably well established from previous experience except for the normal drag coefficient (c_n), which is the coefficient involved in the linearized normal drag term. It is the value of this term that is least certain. The Rispin[6] experiment showed that for shallow attack angles, less than 2.5 to 3 deg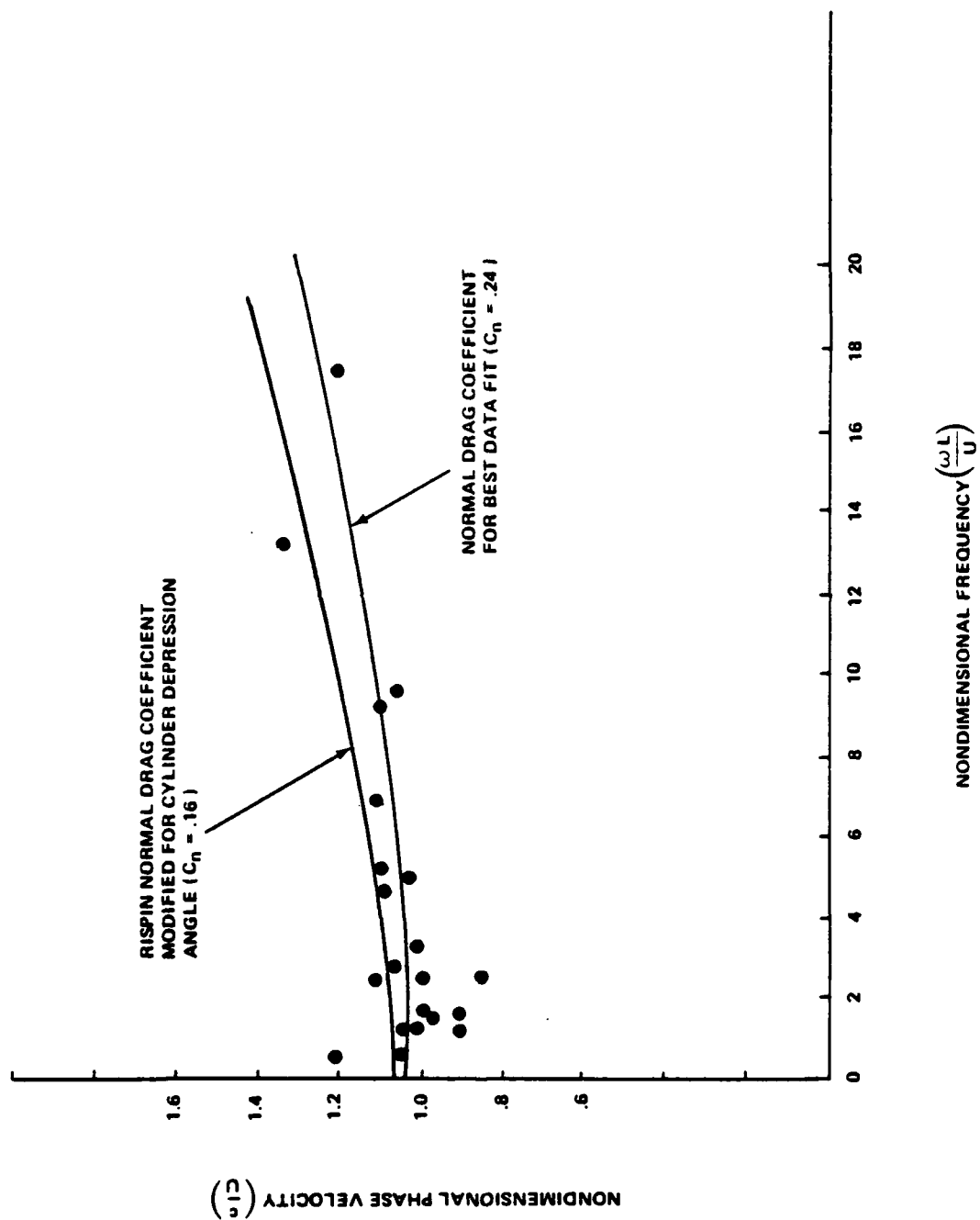rees, the form assumed by Paidoussis was correct and had a coefficient value of c_n equal to .070.* From equation (39) and figure 11 we would anticipate that the effective coefficient (c_n^*) (which accounts for the effect of a steady vertical tow angle), would be two to three times the Rispin coefficient. To test this, we next determined the value of c_n^* that yielded the best visual fit to both the amplitude and phase data (figures 12 and 13) simultaneously. The value found was 0.16 compared with Rispin's value (.070). From equation (39), $c_n^* = 0.16$ implies an effective amplification value of 2.29. This value falls within the independently predicted value range shown in figure 11. The theoretical curves obtained this way are labeled "Rispin Normal Drag Coefficient Modified for Cylinder Depression Angle" in figures 12 and 13. The sensitivity of the complex transfer function to changes in the value of c_n^* was examined during the above curve fitting procedure. It was found that factor of two changes in c_n^* yielded changes in $|H(\omega)|$ and $c*/U$ of less than ± 0.1 in both cases.

The rest of the analytical coefficients are $\varepsilon = 75000$, $c_n = .2020$, $\xi = 1.0$, $\beta = 0.5$, $c_t = .0101$, and $c_t' = 228$.

Other theoretical curves were calculated using two different values of c_n^*; one curve represents the best visual fit to the transfer function magnitude, and the other represents the best visual fit to the nondimensional phase velocity. These are labeled "Normal Drag Coefficient for Best Data Fit" in figures 12 and 13.

Figure 12 shows that use of the Rispin parameter overestimates the measured transfer function magnitude and that a smaller value of c_n is necessary to match the data. Since the only attenuative mechanism available is the normal hydrodynamic drag, which introduces a velocity damping, this result would appear to run counter to intuition. That is, attenuation increases with an increase in normal drag. To see the source of this apparent contradiction, let us recall that the normal drag force is modeled as

$$F_N = \frac{2c_n}{\pi} \frac{M}{d_c} U \left(\frac{\partial y}{\partial t} + U \frac{\partial y}{\partial x} \right)$$

in equation (1), where the flow across the cable is $\partial y/\partial t + U(\partial y/\partial x)$. Presumably an increase in c_n should increase the attenuation for a given frequency. Let us examine the normal force when y is a wave traveling downstream with the phase velocity $c(\omega)$, as expressed by:

---

*This value will be referred to as the Rispin coefficient.

$$y = Ye^{i(\omega t - kx)} \, ,$$

where $k = \dfrac{\omega}{c(\omega)}$.

Then,

$$F_N = \frac{2c_n}{\pi} \frac{M}{d_c} UY\omega \left(\frac{U}{c} - 1\right) e^{i(\omega t - kx)} \, .$$

Thus we see that the phase velocity must be different than U for a damping force to exist. But we recall from the discussion of equation (14) that the phase velocity is proportional to $1 + P^{-1}$. A decrease in c_n is thus needed to increase the attenuation. Likewise, in figure 13, an increase in c_n was necessary to best fit the phase velocity data. The absence of a single value of c_n that best fits both the amplitude and the phase of the measured transfer function illustrates the difficulty of the linear model in matching data.

The data was next examined to determine whether a better fit to the curves calculated using the modified Rispin coefficient would be possible by editing out those runs that had very large θ. The results were negative. Other attempts at observing a nonlinear amplitude effect have yielded similar negative correlations. Presumably a better fit to theory would be possible with a more rigorous handling of the three-dimensional dynamics and a more exact treatment of the nonlinear hydrodynamic normal drag. However, the current theory does agree with experimental values to roughly 25 percent.

SUMMARY

A linear theory describing the transverse motion of a cable being towed by a vessel imperfectly attempting to steer a straight-line course was studied both theoretically and experimentally. The analytical approach was to: (1) expand the existing theory of the transverse motion of neutrally buoyant, long, flexible cylinders in a uniform axial flow, and (2) modify the coefficients of this theory to account for the horizontal-vertical interaction of forces resulting from the steady vertical towing angle associated with the towing of negatively buoyant cables. This approach was taken to avoid the difficult problem of deriving and solving the appropriate governing equation in three dimensions.

The results of the numerical calculations show that for parameters typical of long cables towed at sea, disturbances occurring on the upstream boundary (tow point) propagate dispersively and attenuatively downstream. Both the attenuation and the phase velocity of the disturbance are functions of the frequency content of the disturbance and the distance between the tow point and an observer. These examples served to quantify a physical description of the process previously given by Kennedy.[11] In that description it was shown that at low frequencies, where inertial and tension forces are dominated by hydrodynamic drag terms, the attenuation is small

and the phase velocity is near the fluid flow velocity. Both quantities change little spatially because the hydrodynamic forces are spatially uniform. As the frequency increases enough for the inertial forces and tension forces (because of the increased curvature of the cylinder) to become significant, the attenuation and phase velocities increase and both become spatially dependent as a consequence of the linearly changing tension. The theory developed in this report shows that there are no resonances encountered by excitation by real frequencies.

The temporal stability of these cylinders was also investigated with limited results. A basic low frequency assumption is made throughout this report which limits one's inspection of all Eigenvalues of the system. However, those Eigenvalues that lead to Eigen frequencies within the region for which the present theory applies indicate a temporally stable system. This is thought, in general, to be true because no instabilities have been experimentally observed.

It was shown in this study that if a cylinder is statically inclined vertically as well as dynamically inclined horizontally, there is an effective amplification of the horizontal component of normal force on the cable. This accentuates the hydrodynamic forces and thus causes the "water pulley" effect.[11]

An experiment was performed at sea to test the theory. The parameter values used in the calculations were standard except for the hydrodynamic normal drag term coefficient. Ultimately, the value for the coefficient measured in the laboratory by Rispin[6], amplified to account for the horizontal-vertical interaction of forces discussed above, yielded a solution that fit the data to within 25 percent. We are therefore confident that we had modeled the dominant physical mechanisms. Better individual fits to the magnitude and phase components of the transfer function were possible by changing c_n for each component. The absence of a single value of c_n that best fit both the amplitude and phase of the measured transfer function illustrates the difficulty of the linear model in matching data. A better fit to theory would probably be possible with a more rigorous handling of the three-dimensional dynamics and a more exact treatment of the nonlinear hydrodynamic normal drag.

REFERENCES

1. J. D. Mudie and W. D. Ivers, Simulation Studies of the Response of a Deeply Towed Vehicle to Various Towing Ship Maneuvers, Ocean Engineering, vol. 3, pp. 37-46.

2. M. P. Paidoussis, "Dynamics of Flexible Slender Cylinders in Axial Flow," Journal of Fluid Mechanics, vol. 26, 1966, pp. 717-751.

3. C. R. Ortloff and J. Ives, "On the Dynamic Motion of a Thin Flexible Cylinder in a Viscous Stream," Journal of Fluid Mechanics, vol. 38, part 4, 1969, pp. 713-720.

4. J. S. Tennant and S. E. Dunn, Unpublished Manuscript.

5. G. I. Taylor, Proceedings of the Royal Society, A214, 1952, p. 214.

6. P. P. Rispin, "Normal Drag on Thin Flexible Cylinders at Shallow Angles," to be published.

7. H. P. Pao, "Dynamic Stability of a Towed Thin Flexible Cylinder," Report 69-11, Institute of Ocean Science and Engineering, The Catholic University of America, December 1969.

8. Private communications with Dr. Paul Rispin (NSRDC).

9. H. P. Pao and Q. Tran, "Response of a Towed Flexible Cylinder in a Viscous Fluid," Journal of the Acoustical Society of America (JASA), vol. 53 (5), 1973.

10. S. Gardner and O. Lindeman, "Transverse Forced Vibration of a Flexible Cylinder in Axial Flow," Journal of Underwater Acoustics (USN), vol. 23 (4), 1973, pp. 523-541.

11. R. M. Kennedy, "Low Frequency Transverse Motion Response of Cable Towed Array Systems," NUSC Technical Memorandum No. 93231, Naval Underwater Systems Center, New London, CT, July 1979.

12. G. N. Watson, "A Treatise on the Theory of Bessel Functions," Second Edition, Cambridge University Press, 1966.

13. T. S. Lee and J. A. D'Appolito, "Stability Analysis of the Ortloff and Ives Equation," TASC Technical Memorandum No. 1588-1, 31 March 1980.

14. D. R. Cox, Planning of Experiments, John Wiley & Sons, Inc. NY, 1958.

15. D. Abraham, J. Mingrone, G. dela Cruz, and D. Wagner, "Engineering Implementation of a Towed Cable/Array Dynamic Response Experiment," NUSC Technical Memorandum No. 801013, Naval Underwater Systems Center, New London, CT, 15 February 1980.

TR 6463

16. R. M. Kennedy and R. R. Kneipfer, "Error Characteristics of Transfer Functions Estimated from Finite Length Noise Free Data," NUSC Technical Memorandum No. 813004, Naval Underwater Systems Center, New London, CT, January 1981.

APPENDIX A

SUMMARY OF EXPERIMENTAL PARAMETERS AND RESULTS

Tables A-1 and A-2 summarize the parameters and results of two experiments. Experiments 1 and 2 were performed in April 1979 and May 1980, respectively. The following symbols are used in the tables:

f is forced vibration frequency in mHz,

L is horizontal distance between acoustic pingers in meters,

a is the peak amplitude of the forced vibration in meters,

λ is the wavelength of the forced vibration in meters,

U is the average velocity of the water relative to the cable in meters per second,

c^* is phase velocity measured between the acoustic pingers nondimensionalized by flow velocity, and

$|H|$ is the magnitude of the transfer function between the two sensors.

The major objective of experiment 1, the initial test, was to determine the feasibility of the experimental concept and to develop some experimental procedures. During experiment 1 there was only one tow vessel speed, $U = 3$m/s, and no modifications of that number were applied to account for vertical current shear. By the time the data analysis for the second experiment took place, more accurate ways of determining U and L were available.

Table A-1. Experimental Parameters and Results
for Experiment No. 1

Run No.	f (mHz)	L (m)	H	c	a/λ
1	0.5	1135	0.995	1.042	0.02
2	1.0	1135	0.917	1.034	0.04
3	2.0	1135	0.681	1.046	0.07
4	0.5	635	0.830	0.898	0.02
5	1.0	635	0.736	1.094	0.04
6	2.0	635	0.414	1.083	0.07

Table A-2.   Experimental Parameters and Results
for Experiment No. 2

Run No.	L (m)	a/λ	U (m/s)	f (mHz)	H	c*
1	1186.9	0.0097	3.10	0.97	0.8223	1.00
2	1186.4	0.0195	3.03	2.07	0.3804	1.10
3	1186.0	0.0395	2.98	3.79	0.1075	1.05
4	1185.7	0.0829	2.94	6.84	0.0085	1.18
5	1193.8	0.0065	5.10	0.37	0.9671	1.19
5A	1194.1	0.0065	5.25	1.10	0.8313	0.90
6	1193.9	0.0130	5.18	2.20	0.6004	1.00
7	1193.5	0.0261	5.00	4.39	0.1922	1.10
8	1192.6	0.0533	4.72	8.18	0.0243	1.33
9	1196.0	0.0049	6.35	1.10	0.9916	1.00
10	1195.9	0.0097	6.25	1.96	0.7091	0.97
11	1195.9	0.0195	6.26	4.03	0.3293	1.03
12	1196.1	0.0395	6.45	7.81	0.0727	1.10
16	1193.9	0.0065	5.15	0.97	0.9442	0.84
17	1193.8	0.0130	5.10	2.20	0.5683	1.03
20	597.1	0.0130	5.28	2.32	0.8255	0.96
21	596.9	0.0261	5.15	4.39	0.5759	1.05

APPENDIX B

HORIZONTAL-VERTICAL FORCE INTERACTION AT SMALL HORIZONTAL
INCLINATION ANGLES

Equations (37) and (38) may be combined to give

$$(F_N)_x = -R \left[\frac{\cos^2 \phi (1 - \cos^2 \theta \cos^2 \phi)^{1/2}}{\sin \theta} \right] \cos \theta \sin^2 \theta \quad . \qquad (B-1)$$

A typical operational scenario would have θ vary as a zero mean random variable in both space and time with a maximum value of less than 3 degrees. The depression angle ϕ would have a steady value between 5 and 45 degrees. For this range of θ and ϕ we may approximate equation (B-1) as

$$(F_N)_x = -R \left[\frac{\cos^2 \phi \sin \phi}{\theta} \right] \theta^2 \quad . \qquad (B-2)$$

The interpretation in the text is that the bracketed term of equation (B-2) serves to modify (amplify) R_1 or, more appropriately, c_n from equation (34).

The point is that the singular behavior of the amplifying term near θ equal to zero does not imply a singular behavior in $(F_N)_x$, but rather a modification of its horizontal inclination angle dependence from a θ^2 to a θ dependence. The singularity of equation (38) is the consequence of some mathematical "bookkeeping" resulting from that functional change.

To avoid the singularity in question formally, we could define an effective amplification (A_{EFF}) as

$$A_{EFF} = \frac{E\left[(F_N)_x\right]}{E\left[(F_N)_x|_{\phi=0}\right]} \quad , \qquad (B-3)$$

where E is the expectation operator and θ is a zero mean, normally distributed random variable with a root mean square value of σ_o. The numerator and denominator of equation (B-3) are evaluated from the integrals in

$$E\left[(F_N)_x|_{\phi=0}\right] = \frac{-2R}{\sqrt{2\pi}\,\sigma_o} \int_0^\infty \theta^2 e^{-1/2(\theta/\sigma_o)^2} \, d\theta$$

$$(B-4)$$

$$E\left[(F_N)_x\right] = \frac{-2R \cos^2 \phi \sin \phi}{\sqrt{2\pi}\,\sigma_o} \int_0^\infty \theta e^{-1/2(\theta/\sigma_o)^2} \, d\theta \quad .$$

TR 6463

The integrals of equation (B-4) may be found in integral tables. The results of the integration are then substituted into equation (B-3) to give

$$A_{EFF} = \frac{\cos^2 \phi \sin \phi}{\sqrt{\pi/2} \; \sigma} \; .$$

(B-5)

A comparison of equations (38) and (B-5) shows them to be functionally the same; yet with (B-5) we have avoided the singular problem.

B-2

A LINEAR THEORY OF TRANSVERSE CABLE DYNAMICS AT LOW FREQUENCIES

Robert M. Kennedy and Eric S. Strahan
Submarine Sonar Systems Department
TR 6463
10 April 1981
NAVSEA, Code 63D
UNCLASSIFIED

DISTRIBUTION LIST

<u>External</u>

APL, University of Washington, Dr. D. E. Calkins
BBN, Dr. S. Africk
C&K Associates, C. Campbell
Chase Inc., Dr. D. Chase
Dunn & Associates, Dr. S. Dunn
EG&G/WASC, P. Bullwinkel and P. Galletta, Contract No. N00140-78-C-8196
G&R Associates, S. Gardner
Hydrotronics, Incorporated; G. Desmarais; Contract No. N00140-78-C-8093
      Dr. S. Berlin; Anaheim, California; Contract No. N00140-78-C-8093
Mar, Incorporated; D. Wagner; Contract No. N00140-79-G-9529-0003
NAVSEA (Code 63R, D. Porter, C. Smith, C. Walker)
      (Code 63D, R. Cockerill, D. Early, W. Williams)
      (Code 6361, CDR R. Welsh)
NOSC, Dr. M. Shensa
NSRDC, Dr. P. P. Rispin
TASC, Dr. J. D'Appolito, Contract No. N00140-79-C-6686

<u>Internal</u>

NUSC/NL
<u>Code</u>   10 (Dr. W. Von Winkle)

Code		
10 (Dr. W. Von Winkle)		332 (Dr. R. Menton)
20 (W. Clearwaters)		401 (Dr. J. Patel)
32 (J. Kyle)		721 (R. Bernier)
33 (A. Nuttall)		2212 (D. Fraioli)
101E (Dr. E. Eby)		3122 (Dr. D. Lee)
321 (Dr. J. Kingsbury)		3211 (J. Hall, N. Owsley)
323 (D. Abraham, G. Connally,		3212 (Dr. J. Ianniello, R. Kneipfer)
B. Helme, J. Marsh,		3331 (Dr. J. Beam, Dr. C. Carter)
Dr. H. Schloemer,		7213 (N.L. Library) (3)
Dr. C. Sherman)		7223 (Newport Library)
323M (Lt. D. Wilson)		72254 (Distribution Center) (10)

NUSC/FL
<u>Code</u> 3231 (S. Snyder) (6)

<u>External copies: 21</u>
<u>Internal copies: 44</u>
  Total copies: 65